Biol Cybern (2014) 108:803–823
DOI 10.1007/s00422-014-0625-3

ORIGINAL PAPER

Biological Cybernetics

Torque–stiffness-controlled dynamic walking with central pattern generators

Yan Huang · Bram Vanderborght · Ronald Van Ham · Qining Wang

Received: 21 November 2013 / Accepted: 22 July 2014 / Published online: 16 August 2014

Abstract Walking behavior is modulated by controlling joint torques in most existing passivity-based bipeds. Controlled Passive Walking with adaptable stiffness exhibits controllable natural motions and energy efficient gaits. In this paper, we propose torque–stiffness-controlled dynamic bipedal walking, which extends the concept of Controlled Passive Walking by introducing structured control parameters and a bio-inspired control method with central pattern generators. The proposed walking paradigm is beneficial in clarifying the respective effects of the external actuation and the internal natural dynamics. We present a seven-link biped model to validate the presented walking. Effects of joint torque and joint stiffness on gait selection, walking performance and walking pattern transitions are studied in simulations. The work in this paper develops a new solution of motion control of bipedal robots with adaptable stiffness and provides insights of efficient and sophisticated walking gaits of humans.

Keywords Adaptable joint stiffness · Passive dynamic walking · Controlled passive walking · Central pattern generators · Velocity control · Walking pattern transitions

Y. Huang · Q. Wang (✉)
Intelligent Control Laboratory, College of Engineering, Peking University, Beijing 100871, China
e-mail: qiningwang@pku.edu.cn

B. Vanderborght · R. Van Ham
Department of Mechanical Engineering, Vrije Universiteit Brussel, 1050 Brussels, Belgium

1 Introduction

Stability guaranteed bipedal walking is one of the keys but also one of the more challenging components of humanoid robot design. Investigations on bipedal walking can help better understand the essentials of complex human gaits and build efficient bipedal walking prototypes.

Different from the actively controlled walking which is often found in commercial humanoids, passivity-based dynamic bipedal walking may not reach equilibrium at every moment during motion, but can realize stable cyclic locomotion. Passive dynamic walking (McGeer 1990) has been presented as a possible explanation for the efficiency of the human gait, which showed that a mechanism with two legs can be constructed so as to descend a gentle slope with no actuation and no active control. Several follow-up studies demonstrated these kinds of walking machines work with reasonable stability over a range of slopes (Collins et al. 2001; Suzuki et al. 2005) and on level ground with kinds of actuation added (Collins et al. 2005; Wisse et al. 2007). Recently, studies on passivity-based dynamic walkers with flat feet, which are more similar to humans in morphology, attracted considerable attention (Wisse et al. 2007; Hobbelen and Wisse 2008a; Wang et al. 2010a,b). Compared with the actively controlled walking, passivity-based walking achieves higher efficiency and performs more natural gaits (Collins et al. 2005). However, passivity-based bipeds often has limitations in versatility, such as performing various locomotion modes and completing different tasks (Vanderborght et al. 2008).

Natural bipedal walking is different from the passivity-based walking mentioned above. Humans are able to actively control walking gaits according to different environments and tasks, while keeping efficiency, elegance and simplicity (Perry 1992). Inspired by the natural bipeds, several studies

made efforts to add a certain amount of active control into passivity-based walking to obtain a versatile walker with low energy consumption and controllable walking patterns (Mandersloot et al. 2006; Geng et al. 2006; Hobbelen and Wisse 2008a). Most of these studies achieved velocity control by only adjusting the external energy input, while the intrinsic characteristics (such as the natural frequency and joint compliance) of the walker maintained invariant.

As manifested by previous studies, stiffness plays an important role in energy exchange and modulating walking performance during locomotion of both humans (Kim and Park 2011; Ishikawa et al. 2005) and passivity-based bipedal robots (Wang et al. 2010a; Huang et al. 2012). Actuators with adaptable compliance can exploit the natural dynamics, reduce the energy consumption and extend the versatility (Owaki et al. 2008; Hosoda et al. 2008; Kormushev et al. 2011; Ugurlu et al. 2012). Different types of compliant actuators were designed and applied in robotics (Ham et al. 2009), such as the pneumatic artificial muscles (Vanderborght et al. 2008) and MACCEPA (short for mechanically adjustable compliance and controllable equilibrium position actuator) (Ham et al. 2007). However, in most existing studies on dynamic walking, the stiffness (or compliance) is changed off-line. The transition of different patterns, velocities and step lengths through controlling stiffness in real time was not investigated. Our previous study has demonstrated that a passivity-based bipedal walker with adaptable compliance based on the concept of Controlled Passive Walking (Ham et al. 2007) is able to change the velocity and step length to a desired natural motion by controlling joint compliance in both simulated model and the physical robot (Huang et al. 2013). In this type of walking, the natural dynamics can be adjusted in real time. Nevertheless, it was a relatively preliminary validation without a systematic control method. The respective effects of joint torque and joint stiffness (represent for external input and internal dynamics, respectively) on walking performance, speed control and walking pattern transition were not studied.

The biologically inspired control methods based on central pattern generators (CPGs) can modulate the motion performance (e.g., speed and gait type) smoothly with only a few control parameters (e.g., drive signals) (Ijspeert 2008; Ijspeert et al. 2007), which is suitable for the control of dynamic walking with adaptive stiffnesses and controllable torques. In this paper, we build a human-like passivity-based dynamic walking model with an upper body, flat feet and adaptable compliant joints. A CPG model is presented and applied to controlling the proposed bipedal walker. The CPG-based control approach reduces the control parameters and simplifies the control structure with a natural way. The model has two control parameters for adjusting joint torques and joint stiffnesses, respectively. Thus, the external actuated torques and the natural dynamics can be controlled independently during walking. We name this type of bipedal walking as torque–stiffness-controlled dynamic walking, which expands the concept of controlled passive walking. It is easier to control the locomotion to the desired natural motion with specific walking velocity and step length. In the simulations, we validate the effectiveness of the proposed torque–stiffness-controlled dynamic walking, and study the effects of joint torques and joint stiffnesses, respectively, on walking performance, gait selection and pattern transitions.

2 Dynamic bipedal walking model

2.1 Biped model

To study the walking performance of passivity-based dynamic walking with controllable joint torques and joint compliance, we proposed a seven-link bipedal walking model, which consists of an upper body, two thighs, two shanks and two flat feet. Each leg includes a hip joint, a knee joint and an ankle joint. The proposed bipedal walker travels forward on level ground. A kinematic coupling has been added at the hip to keep the upper body midway between the two thighs, which is similar to former studies (Wisse et al. 2007; Ham et al. 2007). We assume that the friction between the walker and the ground is sufficient, thus the flat feet do not deform or slip. All strikes are modeled as instantaneous, fully inelastic impacts where no slip and no bounce occurs.

Previous studies indicated that the torque–angle relation of human walking is quite similar to that of a torsional spring (Weiss et al. 1986a,b; Frigo et al. 1996). Thus, in lots of passive bipedal walkers, the compliant joints are modeled as torsional springs (Owaki et al. 2008; Hobbelen and Wisse 2008b; Huang et al. 2012). Different types of compliant actuators were also designed and applied in bipedal robots to improve the performance (Ham et al. 2007; Hobbelen and Wisse 2008b; Ham et al. 2009). Actuators with variable stiffnesses can exploit the natural dynamics and reduce the energy consumption (Vanderborght et al. 2009). The control of most variable stiffness actuators can be considered as controlling the equivalent equilibrium position and stiffness (Vanderborght et al. 2013). In this paper, the variable stiffness actuators equipped on each joint are modeled as simple torsional springs with both adjustable equilibrium positions and the spring constants. The joint torques are calculated as follows:

$$T = -k \cdot (\theta - \widetilde{\theta}) - d \cdot \dot{\theta} \tag{1}$$

where T is the joint torque generated by the spring-like actuators, k is the spring constant, θ is the joint angle, i.e., the angle between the two sticks connected at the joint, and $\widetilde{\theta}$ represents the equilibrium position, where the joint torque is zero. d is the damping coefficient. In order to alleviate the oscillatory joint motion, we add a damper to each joint.

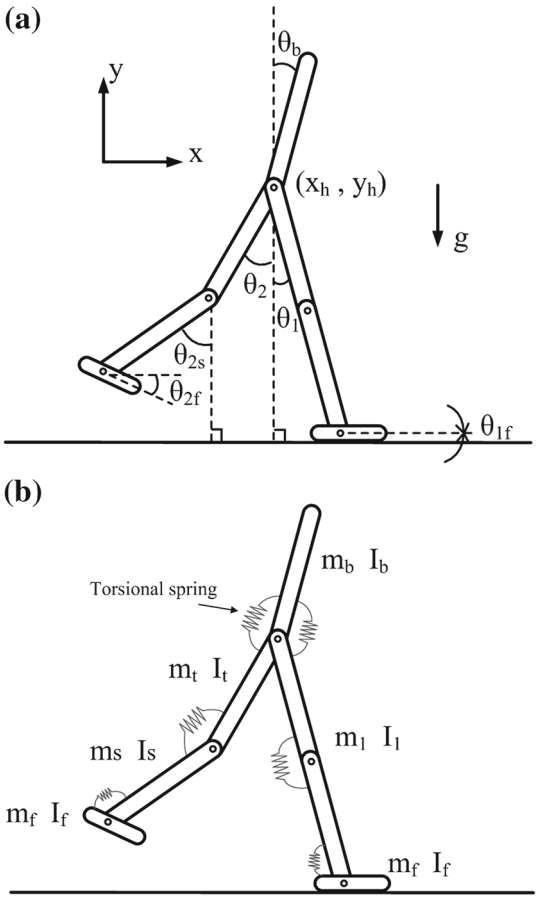

Fig. 1 The seven-link bipedal walking model. The upper body, the legs and the feet are modeled as rigid sticks without flexible deformation. The mass of each part is averagely distributed among the corresponding stick. **a** The degree of freedom, **b** the mass distribution and the torsional springs at the joints

The damping coefficients are set according to the critical damping. $\dot{\theta}$ is the joint angular velocity. Thus, the control parameters of the mechanical system are all the equilibrium positions and spring constants, which determine the torque and stiffness of each joint. Figure 1 shows the structure and the related variables of the biped model.

In this study, we employ a simple and general torsional spring model in order to exploit the essential characteristics of variable stiffness actuators. Thus, the results of this study can be expected to be suitable for a large variety of dynamic bipedal walkers with adaptable stiffness.

2.2 Walking phases

Different from most former passivity-based bipedal walking models with point feet or round feet (Taga et al. 1991; Verdaasdonk et al. 2009; Owaki et al. 2012), the biped model in this paper is mounted with flat feet, which is more close to humans in the structure and walking gaits. Flat-foot walkers have the ability of standing stably and can help us study the effects of foot rotation and ankle compliance in dynamic walking (Wang et al. 2010a; Chevallereau et al. 2008). When the compliant ankle is actuated, as is the case in Meta (Hobbelen and Wisse 2008b), extra energy can be inserted in the toe-off phase (Ker et al. 1988).

In this study, different walking phases are distinguished by the constraint conditions. A walking gait is denoted as the sequence of certain walking phases under a specific order. A walking pattern refers to a limit cycle with specific velocity and step frequency. Thus, different patterns may be realized with the same gait. Different from most of existing studies on passivity-based walking, the series of walking phases is not predefined in this study. The dynamic switching of the walking phases is more close to that of natural human walking.

The walking sequence of the flat-foot walker is more complicated than that of the round-foot walker or point-foot walker (Wang et al. 2010a; Huang et al. 2012). When the flat foot strikes the ground, there are two impulses, "heel-strike" and "foot-strike", representing the initial impact of the heel and the following impact as the whole foot contacts the ground, respectively. Each foot has three contact cases: foot contact, heel contact and toe contact. Thus, there appears three possible human-like gaits, distinguished by the order of three important events: heel-off of the trailing leg, heel-strike of the leading leg and foot-strike of the leading leg.

Figure 2 illustrates the walking phase sequences during one step of these three gaits. All the three gaits start from push-off phases, shown as phase *A* and phase *B* in Fig. 2. In phase *A*, the trailing leg keeps knee-straightening and the shank is constrained to the same direction of the thigh. When the constraint knee torque decreases to zero, the knee joint is unlocked and made compliant, and the walker moves to phase *B*. Phases *C* and *D* are single-stance phases. The difference of the two phases is the direction of the knee torque of the swing leg. The torque bends the knee in phase *C* while stretches the knee in phase *D*. After the knee impact, the constraint on the knee joint of the swing leg is added again and the walker moves to phase *E*, where the motion comes to the bifurcation point. In the case of small joint torques and joint stiffnesses, the heel of the trailing leg will not rise up until foot-strike of the leading leg, and the walker performs gait 1. If the heel rise of the rear leg occurs between the heel-strike and the foot-strike of the front leg, the walking will falls into gait 2. When the ankle torque is large enough, the trailing leg performs heel rise before the swing leg touches the ground, which is called premature heel rise in previous studies (Hobbelen and Wisse 2008b). Then the biped model will move to dynamic walking with gait 3. After foot-strike, the stance leg and the swing leg will be swapped and another walking cycle will begin. Therefore, compared with previous point-foot walkers or round-foot walkers, the proposed

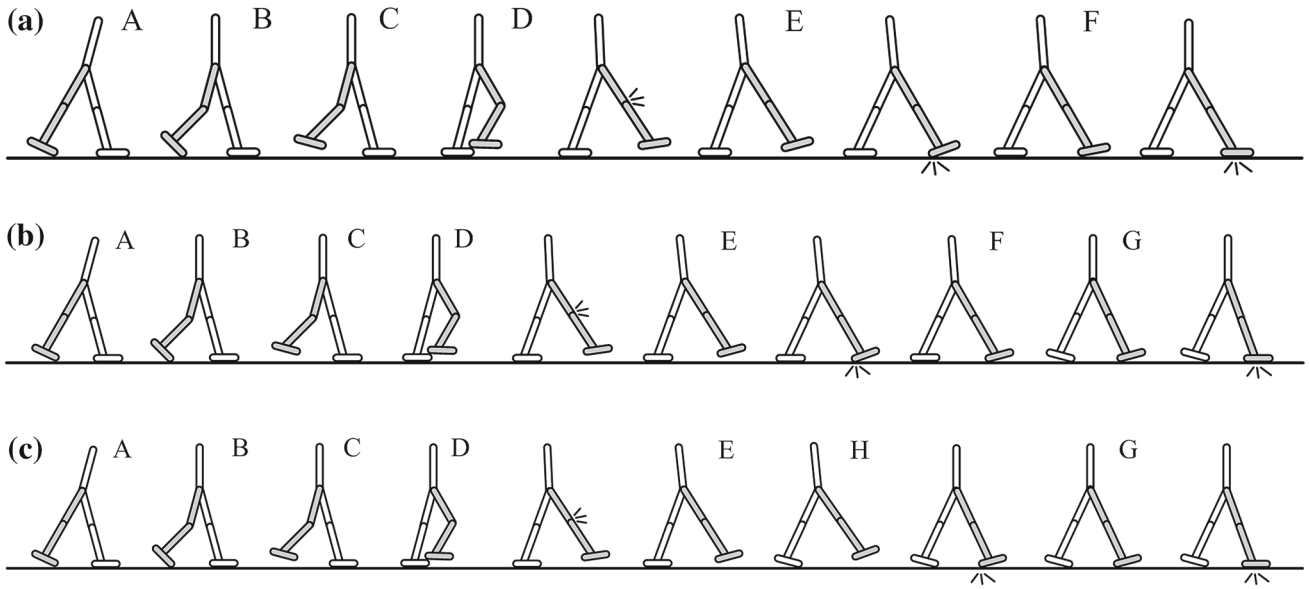

Fig. 2 The schematic diagrams of the three walking gaits of dynamic bipedal walking with flat feet and adaptable compliant joints. **a**, **b** and **c** represent gait 1, gait 2 and gait 3, respectively. Since impacts are instantaneous, only motion phases are marked. One leg is *gray* for clarity

flat-foot walker can realize multiple walking gaits and thus be used to study gait transitions of dynamic bipedal walking.

The equilibrium position and stiffness of each joint are different in different walking phases. If moving to another phase is detected, the control parameters will change to the new set according to the new phase. Phase switching is triggered by foot contact information and certain joint angles. Since the bisecting mechanism equipped at the hip joint restrains the direction of the upper body, the two springs at the hip joints have the same stiffness and opposite equilibrium positions.

2.3 Walking dynamics

The Lagrange's equation of the first kind is used to construct the equations of dynamics. We suppose that the x-axis is along the forward direction while the y-axis is vertical to the ground upwards, as indicated in Fig. 1. The configuration of the walker is defined by the position of the hip joint and the angle of each stick. Thus, the posture of the model can be arranged in a generalized vector:

$$\mathbf{q} = (x_h, y_h, \theta_1, \theta_2, \theta_b, \theta_{2s}, \theta_{1f}, \theta_{2f})'. \quad (2)$$

The superscript $'$ means the transposed matrix (the same in the following paragraphs). The positive directions of all the angles are counter-clockwise. Note that the dimension of the generalized vector in different phases may be different. When the knee joint of the swing leg is locked, the freedom of the shank is reduced and the angle θ_{2s} is not included in the generalized coordinates. Consequently, the dimensions of the mass matrix and the generalized active force are also reduced in some phases. The detailed derivation of the equations of motion and impacts and the mechanical parameter values can be found in "Appendix A". The mechanical parameter values of the biped model are set based on a rough estimation of mass distribution and morphology of humans (Wisse et al. 2007; Wang and Crompton 2004).

3 CPG-based control system

Although other control methods may be applied to the proposed torque–stiffness-controlled dynamic walking, we consider that the bio-inspired CPG-based approach, which can simplify the control structure and reduce the dimension of inputs, is suitable for the biped model with multiple joints and limb coordination.

3.1 Related works

Central pattern generators (CPGs) are considered as neural circuits which can produce coordinated gait patterns of high-dimensional rhythmic output signals while receiving only simple, low-dimensional, input signals (Ijspeert 2008). Studies in neuroscience revealed that CPGs are distributed networks made of multiple coupled oscillatory centers (Delvolve et al. 1999). Several studies have reported evidences of the existence of CPG in vertebrates (Amemiya and Yamaguchi 1984; Cazalets et al. 1995). For many animals, CPGs can produce rhythmic patterns of neural activity and control motion gaits.

Inspired by biological studies, a variety of CPG models have been designed and applied to locomotion control of different types of biomimetic robots, e.g., (Ijspeert et al. 2007; Fukuoka et al. 2013; Kim et al. 2011; Li et al. 2012). Investigation on ZMP-based humanoid robots demonstrated that the walking performance can be improved by adding CPG components to the controller (Or 2009). Several studies tried to introduce CPG-based control methods to passivity-based bipedal models. Taga et al. (1991) implemented adaptive control of a CPG-controlled bipedal walking model and demonstrated the robustness in unpredictable environments with perturbations. Verdaasdonk et al. (2009) applied CPG models to controlling a passive walker with rotational hip stiffness. The results revealed that CPG-based control approach is beneficial in improving walking efficiency and eliminating chaos. Owaki et al. (2012) studied CPG-controlled locomotion of a passive biped model with leg stiffness and hip stiffness. By controlling only one parameter, the model can exhibit walking and running gaits.

Previous studies indicated that CPG-based control methods could enhance robustness against perturbations, improve efficiency, and modulate complex motion behaviors (e.g., speed control or transitions between different gaits) by receiving only a few input signals (Ijspeert 2008). Thus, CPG-based control methods are very suitable for controlling bipeds with adaptable stiffness and walking pattern transitions. In this paper, we introduce real-time stiffness control to CPG. The CPG model controls not only the joint torque but also the joint stiffness, which is different from most existing studies on CPG-controlled bipedal walking. In former research on passivity-based bipedal walking, the higher center usually generates only a single driven signal for tuning the basic rhythm of joint torques (Owaki et al. 2012; Verdaasdonk et al. 2009; Taga et al. 1991). The novelty in this paper is the addition of another input signal for the adjustment of joint stiffness in bipedal walkers. The natural dynamics such as the velocity and the step frequency can be controlled by adjusting joint stiffness.

3.2 Control architecture

In this paper, the torques acted at joints for the actuation is called as external actuation, while the structural properties such as joint stiffness and natural limb frequency are considered as internal natural dynamics. For controlling gait performance through tuning both external actuation and internal natural dynamics, the input of the control system in this study is the desired walking pattern while the outputs (i.e., the commands sent to musculo-skeletal system) are joint torque and joint stiffness. The control system receives feedbacks from the motion states of the walker and the interaction between the mechanical system and environments. The architecture is shown in Fig. 3.

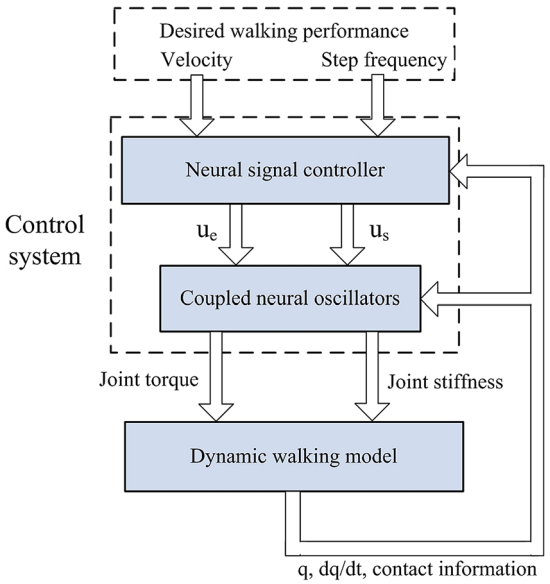

Fig. 3 The diagram of the control scheme. The control system receives the expected walking performance and sends commands as joint torque and joint stiffness to the mechanical system. The sensory feedback is from the motion states of the walker to both the neural signal controller and the coupled neural oscillator

The performance of different walking patterns is evaluated by velocity and step frequency. Different from most previous studies which control only the speed, the CPG model in this paper is expected to control both velocity and step frequency simultaneously. Thus, the walking behavior can be modulated over a wider range by controlling natural dynamics. In this study, step length is defined as the increment of the x-coordinate of the hip joint from a foot-strike to the next foot-strike. Walking velocity of each step is calculated by dividing the step length by the time duration between two consecutive foot strikes.

The control system consists of a neural signal controller and coupled neural oscillators. The neural signal controller generates appropriate signals u_e and u_s according to the desired and the actual walking performance. The two parameters u_e and u_s are responsible for adjusting the equilibrium position and the stiffness of each joint, respectively. Therefore, controlling u_e changes only the joint torques with fixed joint stiffness, while controlling u_s changes stiffnesses and thus torques. The coupled neural oscillators provide rhythmic patterns of joint torques and joint stiffnesses. The motion of each joint is stimulated by two unit oscillators, for inducing equilibrium position and stiffness, respectively. The coupled neural oscillators are composed of twelve coupled unit oscillators, associated with walking phase-dependent sensory feedback from the motion states (i.e., the generalized coordinates and velocities) and foot contact information. Similar to Owaki et al. (2012), interaction among different joints contains both inter- and intra-limb coordination.

3.3 Neural signal controller

A neural signal controller is designed to update the signals u_e and u_s for realizing real-time walking pattern transitions according to the variance of desired walking pattern. The controller can also improve the robustness against disturbances.

If only one walking criterion, for example the velocity, is specified a desired value, the control can be implemented by changing each of u_e and u_s or both the two. In this study, these three control methods are denoted as method-I (control only u_e with fixed u_s), method-II (control only u_s with fixed u_e) and method-III (control both u_e and u_s), respectively. The control rule is designed as follows:

$$u(n+1) = \begin{cases} u(n) + G_p(V_{\text{des}} - V(n)), & n = 1 \\ u(n) + G_p(V_{\text{des}} - V(n)) & \\ \quad + G_d(V(n-1) - V(n)), & n \geq 2, \end{cases} \tag{3}$$

where V_{des} is the desired velocity, $V(n)$ is the velocity of the nth step, G_p and G_d are gain coefficients, and $u(n)$ denotes u_e (method-I), or u_s (method-II), or both u_e and u_s (method-III) of the nth step. In method-III, we empirically choose a combination that the two parameters increase or decrease proportionally, satisfying the following constraint:

$$u_e(n+1) - u_e(n) = a \cdot (u_s(n+1) - u_s(n)), \quad n \geq 1, \tag{4}$$

where a is a constant coefficient.

The control rule shown by Eq. (3) is analogous to increment proportional-derivative (PD) control. The proportional term is for restraining the error, while the derivative term is important for detecting the tendency of error and preventing too large maximal deviation, which is necessary owing to the hysteretic effects of the variation of u_e or u_s on walking gaits of passivity-based bipeds. Increasing G_p can help the velocity or step length converge. However, too large G_p may lead to unstable gaits. A appropriate G_d can prevent u_e and u_s from changing too fast, which is helpful in reducing the oscillatory behaviors. a is used to adjust the portions of equilibrium position control and stiffness control in controlling velocity. In this study, in method-I $G_p = 0.25,\ G_d = 0.25$, in method-II $G_p = 7,\ G_d = 1.5$, and in method-III $a = 0.017$ and $G_p = 0.1,\ G_d = 0.02$ for u_e while $G_p = 6,\ G_d = 1.2$ for u_s.

In the case that the walking pattern is modulated by controlling both velocity and step frequency, both u_e and u_s have to be changed during the transition. The control rule is designed as:

$$\begin{aligned} u_e(n+1) &= u_e(n) + G_p(V_{\text{des}} - V(n)) \\ &\quad + G_d(V(n-1) - V(n)) \end{aligned} \tag{5}$$

$$\begin{aligned} u_s(n+1) &= u_s(n) + G_p^s(f_{\text{des}} - f(n)) \\ &\quad + G_d^s(f(n-1) - f(n)) \end{aligned} \tag{6}$$

where G_p^s and G_d^s are the gain coefficients for frequency control. f_{des} and $f(n)$ are the desired frequency and the step frequency of the nth step, respectively. The other variables have the same meanings as in Eq. (3). In this study, the parameter values are set as $G_p = 0.05,\ G_d = 0.02,\ G_p^s = 15,\ G_d^s = 4$. Although each of the two control parameters u_e and u_s may affect both velocity and frequency, the walking gait can fall into a small region around the desired pattern under alternately control actions of Eqs. (5) and (6) with appropriate parameters. The values of the gain coefficients are chosen manually in this study. Note that the optimal parameter values may be changed when the controller is applied to a physical bipedal robot, according to the specific design details. However, the qualitative tendencies of motion control can be preserved.

3.4 Coupled neural oscillators

The coupled neural oscillators receive input signals u_e and u_s and output rhythmic joint torques and stiffnesses, to generate periodic stable gaits. The control system contains twelve unit oscillators. Each joint is controlled by two unit oscillators, producing the equilibrium position and stiffness, respectively. Since the above mentioned kinematic coupling at the hip to keep the upper body midway, the stiffness will be set equal for both the two hip joints, and the equilibrium position will be set opposite. Due to this reduction, there are actually only ten independently unit oscillators. However, to make the control architecture close to the physical structure of the biped, we keep the form of twelve unit oscillators in the rest of this paper. The connections between the unit oscillators and the feedbacks from the state variables of the biped and the foot contact information are expected to represent the general bipedal walking characteristics among various walking gaits. Thus, walking pattern can be controlled simply by changing the two parameters u_e and u_s.

In order to study the respective effects of joint torque and stiffness, the interaction terms of the unit oscillators for equilibrium control do not include coupling with the unit oscillators for stiffness control, and vice versa. Inter-limb coordination between the two legs is established between the hip unit oscillators on the contralateral side. Inhibitory connection of equilibrium positions results in phase difference between hip angles and thus form periodic motions. Intra-limb coordination makes the stiffnesses of ipsilateral joints increase or decrease proportionally. The structure of the coupled neural oscillators is shown in Fig. 4.

The equations of the unit oscillator model are adapted from the work of Taga et al. (1991). A unit oscillator controlling the joint equilibrium position can be mathematically represented by the following equations:

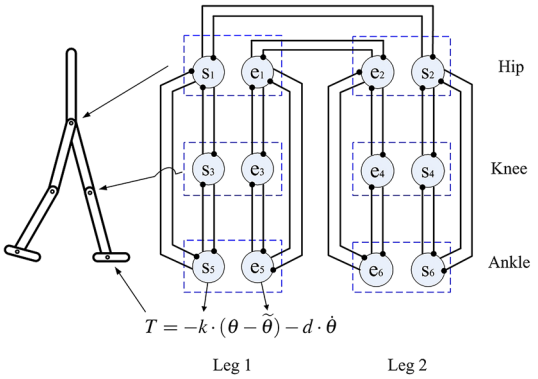

Fig. 4 The schematic diagram of the coupled neural oscillators. The neurons marked with "*e*" is for equilibrium position control, while the neurons marked with "*s*" for joint stiffness control. The outputs of the coupled neural oscillators to the mechanical system are the equilibrium angle and stiffness (thus the torque and stiffness) of each joint as shown in the figure

$$
\begin{aligned}
\dot{u}_i &= \frac{1}{\tau_i}\Big(c_i \cdot \tilde{u}_i^e - u_i + \sum_{j,j\neq i} w_{ij}(\widetilde{\theta}_j + d_{ij} \cdot \widetilde{\theta}_i) - \beta v_i \\
&\quad + F_{eed,i}(q, \dot{q})\Big) \\
\dot{v}_i &= \frac{1}{\tau_i^{'}}(-v_i + \widetilde{\theta}_i) \\
\widetilde{\theta}_i &= \begin{cases} \pi/2, & u_i > \pi/2 \\ u_i, & -\pi/2 \le u_i \le \pi/2, \\ -\pi/2, & u_i < -\pi/2 \end{cases} \quad i = 1, 2 \cdots 12
\end{aligned} \tag{7}
$$

where i is the index of the joints (see Fig. 4); u_i and v_i are state variables; $\widetilde{\theta}_i$ is the output of the unit oscillator, i.e., the equilibrium position; $\tilde{u}_i^e$ is the input signal, which is equal to u_e or $-u_e$ or a constant, depending on the specific joint and the walking phase; τ_i and $\tau_i^{'}$ are time constants for equilibrium position control; β is the coefficient of adaptation effect for equilibrium position control; c_i is a signal coefficient; d_{ij} is a coefficient to adjust the coordination among different joints; w_{ij} is the connection weights; and $F_{eed,i}$ is the feedback from the motion states of the walker to the unit oscillator for equilibrium position of joint i. The output is constrained in the range from $-\pi/2$ to $\pi/2$. The parameter values and the expressions of feedback are listed in "Appendix B".

The unit oscillator controlling the joint stiffness is given by the following equations:

$$
\begin{aligned}
\dot{u}_i^s &= \frac{1}{\tau_i^s}(c_i^s \cdot \tilde{u}_i^s - u_i^s + \sum_{j,j\neq i} w_{ij}^s(k_j - d_{ij}^s \cdot k_i) - \beta^s v_i^s \\
&\quad + F_{\text{eed},i}^s(q, \dot{q})) \\
\dot{v}_i^s &= \frac{1}{\tau_i^{'s}}(-v_i^s + k_i) \\
k_i &= \max(0, u_i^s)
\end{aligned} \tag{8}
$$

The variables of the oscillators controlling stiffness are marked with a superscript "*s*". These variables have similar meanings with those in Eq. (7). u_i^s and v_i^s are the state variables; k_i represents the stiffness of joint i; $\tilde{u}_i^s$ is the input signal, which is equal to u_s; τ_i^s and $\tau_i^{'s}$ are time constants for joint stiffness control; β^s is the coefficient of adaptation effect for stiffness control; c_i^s is a signal coefficient; d_{ij}^s is a coefficient to adjust the relation among the stiffness of different joints; w_{ij}^s is the connection weights and $F_{\text{eed},i}^s$ is the feedback to the unit oscillator for stiffness of joint i. The parameter values and the expressions of feedback are also listed in "Appendix B".

Note that the expression and parameter values of each unit oscillator are different for different walking phases. Therefore, the CPG model can adjust its frequency with the gait period of the biped, and thus performs rhythmic patterns accompanied with the walking cycles.

Derivative feedbacks of hip and ankle angles are added to the coupled neural oscillators for decreasing time delay effects and preventing the limb moving too fast to maintain stable walking. The unit oscillator for controlling equilibrium position of the knee joint of the swing leg receives feedback from the amount of foot clearance. The knee torque of the swing leg adapts to the current leg posture to avoid foot scuffing by as low energy consumption as possible. The existence of foot rotation is an important difference between flat-foot walkers and round- or point-foot walkers. Former studies indicated that ankle joint plays a significant role in providing power (Kuo et al. 2005). Thus, we particularly focus on the feedback of ankle stiffness. The unit oscillator for ankle stiffness of the stance leg receives sensory feedback from the ankle joint angle and angular velocity. The stiffness increases adaptively in dorsiflexion, which is consistent with the general tendency of human normal walking (Frigo et al. 1996). All these principles of feedback mentioned above are appropriate for different gaits, velocities and step lengths. Thus, flexible walking pattern transitions can be realized by just tuning u_e and u_s.

4 Experimental results

The experiments in this paper focus on the independent effects of joint torque and joint stiffness with a bio-inspired control system. The velocity and step frequency are expected to be controlled independently without coupling. Since step length is more visualized than step frequency and comparing simulated walking with human motion in step length is more convenient than in step frequency, we use walking velocity and step length (equivalent to velocity and step frequency, since step length is the ratio of velocity to frequency) as the performance criteria in experiments. We investigate multiple gaits (gait 1, 2 and 3 in Sect. 2) which result from the flat-foot structure. Velocity, step length, efficiency, gait distribu-

tion and pattern transitions of the proposed torque-stiffness-controlled dynamic walking are studied with adaptable external actuation and natural dynamics.

Since the level of joint torque and joint stiffness are determined by the values of u_e and u_s, respectively, the two input signals u_e and u_s are our main concerned control parameters in the experiments. In this study, u_e changes in the range from 0.21 to 0.45, while u_s in the range from 16 to 37. Larger u_e stands for larger actuation torques, especially the ankle torques in push-off phases and the hip torques in singe-support phases. Increasing u_s makes the joints stiffer. All simulations and data processing were performed using MATLAB 7 (The MathWorks, Inc., Natick, MA) based on the EoMs mentioned in "Appendix A".

4.1 Walking gait distribution

In simulation of the proposed locomotor system, stable walking cycles of different gaits are realized with appropriate parameters. The results indicate that gait 1 has the minimal step length while gait 3 has the maximal step length. In gait 1, heel rise of the rear leg occurs at the moment of foot-strike of the leading leg. The occurrence of heel rise is between heel-strike and foot-strike of the front leg in gait 2. In gait 3, heel rise appears in singe-support phases before the swing leg contacts the ground, which is called "premature heel rise" in previous studies (Hobbelen and Wisse 2008b).

Several former research have studied different gaits of both trajectory-control walkers (Tlalolini et al. 2009) and passivity-based walkers (Huang and Wang 2012) with flat feet. Our previous study compared the motion characteristics of different gaits and showed that ankle stiffness is important in gait selection (Huang et al. 2012). In this paper, we explore the effects of the two control parameters u_e and u_s on gait selection. Heel rise occurs if the ankle torque is high enough to lift the stance leg, thus large u_e and u_s lead to early heel rise. Gait distribution for different input signals u_e and u_s is shown in Fig. 5, which indicates that small u_e leads to gait 1, while gait 3 is concentrated in the area with both large u_e and u_s. Gait 2 is distributed between gait 1 and gait 3. In certain extreme conditions, the bipedal walker performs hybrid gaits (see "gait 1 and 2" and "gait 2 and 3" in Fig. 5). Two different gaits alternatively appear in different steps of the walking, which usually appears in the transitional region between two gaits.

Biological studies indicated that pushing off of the trailing leg begins slightly before the leading leg touches the ground (Kuo et al. 2005). Thus, locomotion around the boundary between gait 2 and gait 3 in the $u_e - u_s$ plane in Fig. 5 is the closest to human normal walking. Our previous research (Huang et al. 2012) has demonstrated that the gaits which are more close to human normal walking have better performance in efficiency.

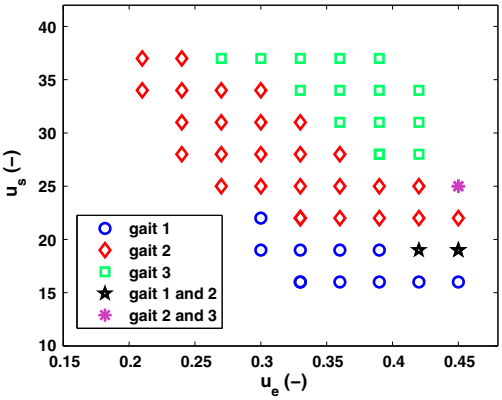

Fig. 5 Gait distribution in the $u_e - u_s$ plane. "gait 1 and 2" and "gait 2 and 3" represent hybrid gaits, in which two different gaits alternatively appear in different steps

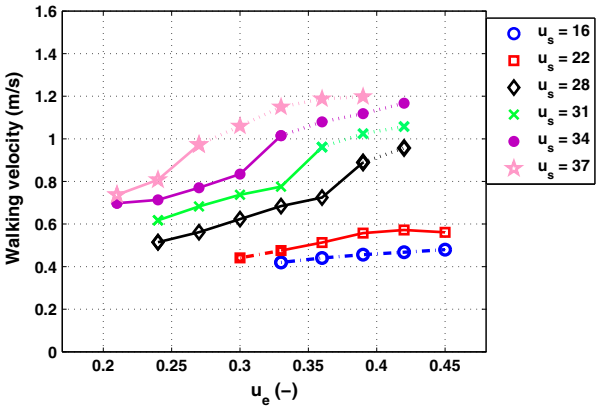

Fig. 6 Walking velocity for varying control parameters u_e and u_s. The *dot-dash line*, *solid line* and *dashed line* represents gait 1, gait 2 and gait 3, respectively,

4.2 Effects of joint torque and joint stiffness on walking performance

In this sub-section, we show the walking performance by variation of control parameters. Figure 6 describes walking velocity with different u_e and u_s. The general tendency indicates that increasing either u_e or u_s leads to forward acceleration, since larger values of u_e and u_s corresponds to more energy input. When u_s is not larger than 22, the locomotion performs gait 1 or gait 2 and the velocity is quite small below 0.6 m/s. In the case that u_s ranges from 28 to 37, stable periodic walking can be obtained with relatively small u_e and gait 3 appears. Increasing u_s can decrease the threshold for u_e of the occurrence of gait 3. The normalized Froude number (defined as $Fr = V/\sqrt{gl}$, where V is the velocity, g is the gravitational acceleration and l is the leg length) can be used to quantify walking velocity (Hobbelen and Wisse 2008a). The obtainable velocity of the proposed biped model ranges from 0.42 to 1.20 m/s. The corresponding range of Fr is from 0.15 to 0.43.

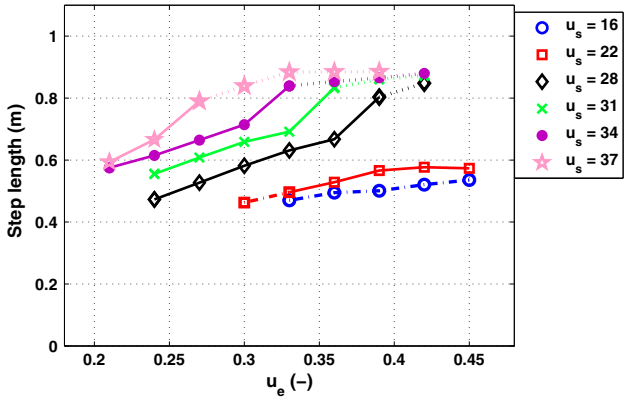

Fig. 7 Step length for varying control parameters u_e and u_s. The *dot-dash line*, *solid line* and *dashed line* represents gait 1, gait 2 and gait 3, respectively,

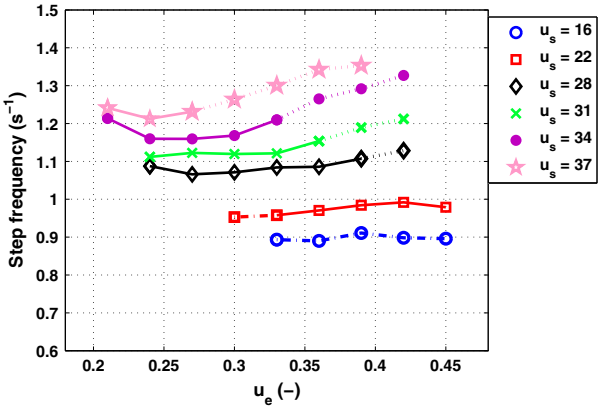

Fig. 8 Step frequency for varying control parameters u_e and u_s. The *dot-dash line*, *solid line* and *dashed line* represents gait 1, gait 2 and gait 3, respectively,

The effects of u_e and u_s on step length are similar with those on velocity. Large u_e and u_s result in large step length. It is worth noting that the step length grows slowly with increasing u_e after reaching a relatively large value, and falls into a small range around 0.88 m (1.1 times leg length). When the walker performs long-step-length walking, large u_e makes the equilibrium position of the hip angle exceed the actual hip angle greatly. The most forward position of the swing leg is difficult to continue moving forward with increasing u_e, since the time delay effects. For long-step-length walking, increasing u_e primarily influences the angular velocity of the swing leg, while only has a minimal influence in step length (Fig. 7).

Step frequency can be obtained as the ratio of velocity to step length. The variation of step frequency for different control parameters is shown in Fig. 8. For the motions with small and moderate step lengths, most in the cases of gait 1 and gait 2, step frequency has almost no dependence on the signal u_e, since the tendencies of velocity and step length are similar with varying u_e. Hence joint torque has little influence in step frequency. This result is consistent with previous studies on passive walkers. For example, Kuo et al. (2005) reported that the walking period is almost invariant with respect to the energy input and the increase in velocity results mainly from increasing step length. Different from the joint torque, joint stiffness is the primary determinant of frequency. As Fig. 8 shows, large u_s leads to high step frequency. For the motions with large step lengths, which often appear in gait 3, the frequency shows obvious dependency on u_e. With increasing u_e, the velocity increases while the step length stays at about the same level. Therefore, the change of velocity results mainly from the variation of step frequency in this case. Tuning either joint torque or joint stiffness is effective for adjusting step frequency in long-step-length walking.

Similar to previous studies on passivity-based walking (Collins et al. 2005; Hobbelen and Wisse 2008a), energetic

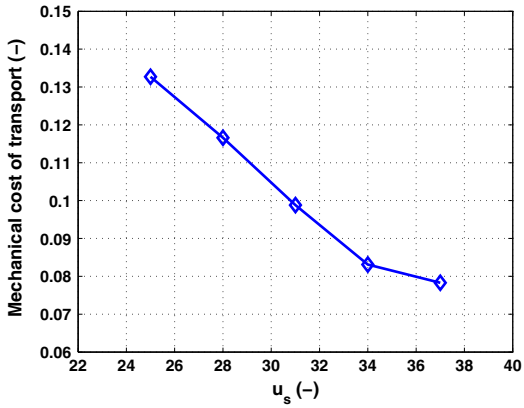

Fig. 9 Mechanical cost of transport of different u_s with equal velocities. The walking velocity stays at 0.73 m/s. The corresponding Froude number is 0.26

efficiency in this paper is measured by the dimensionless mechanical cost of transport c_{mt}, defined as

$$\text{(energy used)}/\text{(weight} \times \text{distance travelled)}.$$

In this study, the energy consumption refers to the active mechanical work. As the joint torques of the proposed model are realized by torsional springs, which store and release energy, certain positive work and negative work counteract each other and hence the amount of active work is reduced. The active work contributes to the increment of elastic potential energy by adjusting the equilibrium position and stiffness of each joint. Figure 9 expresses the efficiency of the proposed model for varying u_s at a constant velocity of 0.73 m/s ($Fr = 0.26$), which is close to human normal walking velocity. The mechanical cost of transport c_{mt} decreases monotonously from 0.13 to 0.078 as u_s increases from 25 to 37. It is worth noting that too large stiffness of the proposed dynamic model may result in serious oscillation and unstable gaits, which is also found in Hobbelen and Wisse (2008b). Thus,

the joint stiffness discussed in this study is in a relatively small range. For the relationship between joint stiffness in the studied range and the energy efficiency (see Fig. 9), one possible explanation is that increasing joint stiffness can decelerate the leg angular velocities just before heel-strike and foot-strike, and thus reduce the energy loss at impacts and improve walking efficiency. Similar results were reported in bipedal walking with actuation and passive springs on ankle joints (Hobbelen and Wisse 2008b).

4.3 Walking stability analysis

In this study, similar to Wisse et al. (2007), walking stability is quantified by the eigenvalues of the Jacobian of the stride map, which indicate the trend of the accumulated errors of each step. Suppose S is the stride function, which represents the mapping from the initial conditions from one step to the next step. Thus,

$$\mathbf{v}_{n+1} = S(\mathbf{v}_n), \tag{9}$$

where $\mathbf{v}_{n+1}$ and $\mathbf{v}_n$ are the initial conditions of the $(n+1)$th step and the nth step, respectively. For the period-1 cyclic motion, the vector of the initial conditions is a fixed point of the stride function.

$$\mathbf{v}_f = S(\mathbf{v}_f). \tag{10}$$

The Jacobian can be obtained by the linearization of the stride function at the fixed point.

$$J_s = (S(\mathbf{v}_f + \Delta\mathbf{v}) - S(\mathbf{v}_f))/\Delta\mathbf{v}, \tag{11}$$

where J_s is the Jacobian of the stride function. $\Delta\mathbf{v}$ is a small perturbation. If the moduli of all the eigenvalues are smaller than 1, the errors decrease step after step and the fixed point is stable.

Figure 10 shows the maximal modulus of the eigenvalues of the Jacobian in the parameter range with obtainable cyclic motions. It is difficult to find periodic gaits at larger or smaller u_e and u_s out of the studied range.

In general, the model has satisfactory performance on stability, especially with moderate u_e and u_s. The walker can handle some disturbance with suitable joint torque and stiffness. However, the stability becomes poor at the edge of the studied parameter region. The moduli of eigenvalues exceed 1 when u_e and u_s have high values, because too large actuation leads to period-2 walking and chaotic gaits, which have negative effects on stability. Another case of low stability is the combination of small u_e and large u_s, for example, the modulus of eigenvalue achieves 3.5 when $u_e = 0.21$, $u_s = 37$. The results indicate that large joint stiffness while relatively small joint torque results in unstable walking. One possible reason is that bipedal walking with high step frequency and small step length may be more sensitive to small perturbations. It may suggest the importance of appropriate coordination between joint torque and joint stiffness for walking stability.

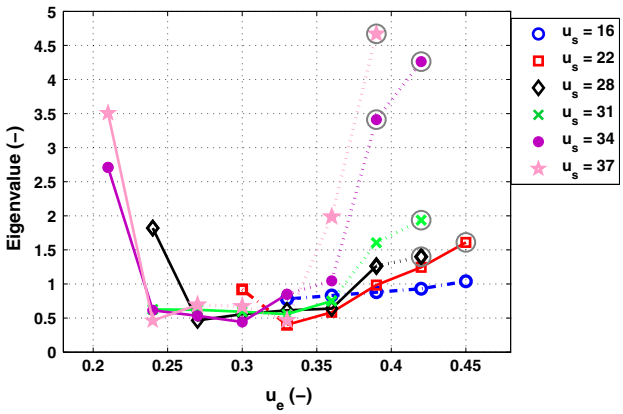

Fig. 10 The maximal modulus of the eigenvalues of Jacobian for varying control parameters u_e and u_s. The *dot-dash line*, *solid line* and *dashed line* represents gait 1, gait 2 and gait 3, respectively. The *gray circles* indicate period-2 motions

4.4 Different velocity control methods

In the following paragraphs, we will show the experimental results of real-time walking pattern transitions. The motion is adapted toward the desired walking performance by controlling the two input signals u_e and u_s.

Walking velocity is usually adopted as the control objective in bipedal walking (Hobbelen and Wisse 2008a; Verdaasdonk et al. 2009). Thus, velocity control of the presented locomotor system is studied in this sub-section. As illustrated in Sect. 3.3, the velocity control can be achieved by method-I, method-II or method-III. Before the transition, the biped model performs stable walking at the velocity of 0.46 m/s ($Fr = 0.164$). At the end of the third step, the desired velocity changes to 0.63 m/s ($Fr = 0.225$). The transition starts at the fourth step and the two control parameters u_e and u_s begin to vary according to the control lows presented in Sect. 3.3.

The walking velocities of each step for the three control methods are shown in Fig. 11a. Method-I produces the fastest responses to the varying desired velocity. However, the rise time of this control method is the longest. The motion does not enter the relative steady state until the thirteenth step. In addition, the velocity shows oscillatory characteristics during the transition. The transition motion with method-II is quite insensitivity to the change of desired velocity. In this case, the rise time is shorter. Steady state is achieved after the eleventh step with satisfactory control precision. Method-III combines the advantages of the two former methods. The velocity rises rapidly at the beginning of the transition and converges to the desired value quickly. The transition is basically completed at the seventh step. All the three methods

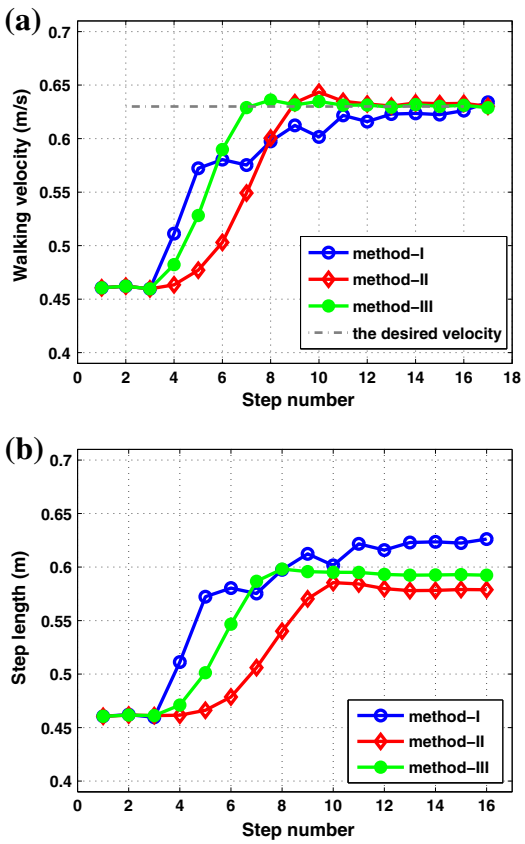

Fig. 11 Walking velocity control of the three different methods. **a** the variation of velocity, **b** the variation of step length during the velocity control. The desired velocity is changed from 0.46 to 0.63 m/s at the end of the third step. The *three solid lines* describe the velocities or the step lengths of each step of the three control methods, respectively. Method-I, method-II and method-III represent changing only u_e, changing only u_s and changing both u_e and u_s, respectively. The *gray dot-dash line* in **a** represents the target velocity

have acceptable control precision, although the accuracy of method-I is slightly worse than those of the other two methods. Comparison of the three control methods indicates that walking performance is more sensitive to the external actuation than to the internal dynamics. The effects of adjusting joint stiffness exhibit in the motion characteristics with a large delay. Moreover, adding joint stiffness control can improve the control precision. In sum, changing both u_e and u_s is the optimal in sensitivity, convergence speed and control accuracy.

The step lengths after the transition of the three control methods are different (see Fig. 11b). A larger portion of adjusting joint stiffness in the velocity control leads to a higher step frequency and thus a smaller step length at the end. The responses of the step lengths of the three methods are similar to the corresponding responses of velocities. Method-I has the maximal final step length. The step length increases rapidly in the early period of the transition while achieves the relatively steady state after a long time. Method-II results in the minimal final step length. The variation of step length still shows insensitive characteristics. The step length of method-III reaches the stable state in the shortest time, which is similar to the case of velocity. The results of step length variation imply that the proposed biped model can realize different walking patterns with the same desired velocity. Adjusting the proportions of u_e and u_s [tuning the coefficient a in Eq. (4)] in velocity control can change the frequency and step length of the expected walking cycle with the same desired velocity.

Table 1 shows the mechanical costs of transport during the transition periods of the three control methods. The period of transition is denoted as the time duration from the step just before changing desired velocity to the step when the difference between the actual and the desired velocities maintains less than 0.003 m/s. This result is consistent with the effects of u_s on efficiency as shown in Fig. 9. Method-II leads to the highest average joint stiffness during the velocity transition and results in the least energy loss at impacts. Thus, method-II is the most efficient method. Contrarily, in method-I, the joint stiffness keeps a relatively low level all the time and the efficiency is the lowest. Method-III has the middle efficiency.

4.5 Walking pattern control

Since the control system in this study introduces joint stiffness control, the walking velocity and step frequency can be controlled simultaneously. Thus, walking pattern transitions can be realized by controlling both u_e and u_s. Equations (5) and (6) are employed as the control law.

The velocity control in Sect. 4.3 is realized with the same gait (gait 2). In walking pattern control, the difference between the initial and the objective patterns can be increased to achieve real-time gait transitions.

Table 1 Mechanical cost of transport of velocity transition of different control methods

Control method	Initial velocity (m/s)	Final velocity (m/s)	Average velocity (m/s)	Step number	Walking distance (m)	Energy consumption (J)	c_{mt}
Method-I	0.460	0.633	0.592	15	8.58	209.97	0.102
Method-II	0.460	0.632	0.557	10	5.23	96.38	0.077
Method-III	0.460	0.632	0.56	7	3.76	77.64	0.086

The motion with increasing velocity and step length starts at the velocity of 0.56 m/s and the step length of 0.53 m. At the end of the third step, the desired velocity and step length are changed to 1 m/s and 0.8 m, respectively. Thus, the expected step frequency is changed from 1.05 to 1.25 s^{-1}. At the end of the twelfth step, the desired velocity and step length return to 0.56 m/s and 0.53 m, respectively. The variations of walking velocity, step length and the two input signals u_e and u_s are indicated by Fig. 12.

Both the velocity and step length track the desired curves with acceptable precision. After the seventh step, the velocity and step length stay within small ranges around the desired values till the objective pattern changes again. Gait switching occurs at the sixth step. The ankle joint torque exceeds the threshold value of premature heel rise by increasing u_e and u_s. The walker performs gait 3 rather than gait 2 after that. At the twelfth step, the walker begins to perform the pattern transition with decreasing velocity and step length. The biped reaches relatively stable states after the nineteenth step. Gait switching occurs at the fourteenth step. The walker performs gait 2 rather than gait 3 after that. Finally, the velocity and step length converge to 0.54 m/s and 0.5 m, respectively. The steady error of walking gait transition is also a little larger than velocity control. This result can be explained by that changing each of u_e and u_s can affect both walking velocity and step length, thus Eqs. (5) and (6) are not completely uncoupled. However, the steady errors are still acceptable.

Figure 12c, d describes the variations of the two control parameters u_e and u_s during walking pattern transitions. The curves of u_e and u_s show a resemblance to those of velocity and step length, which indicates the effects of the two signals on walking performance. The change of u_s exhibits more oscillatory behaviors since step frequency is more sensitive during walking gait transitions (Fig. 10).

Figure 13 shows the stickgram of the walking pattern transitions. The motion characteristics change rapidly around the moment of gait switching.

5 Discussion

5.1 Different walking gaits

In this study, the passivity-based bipedal locomotion is investigated among three different walking gaits. Actually, not all the possible gaits are discussed in Sect. 2.2. For example, when the ankle stiffness of the leading leg in phase *G* is large enough, toe-off of the trailing leg may occur before footstrike of the leading leg. Thus, the walker skips phase *A* and *B* and moves to phase *C* directly. This kind of gaits without push-off phases is rarely observed in normal human walking. In our previous study (Huang et al. 2012), the motion characteristics of all the possible gaits were studied and the results showed that the gaits which are more close to human walking achieve better performance. Studies on gait comparison of active walkers (Tlalolini et al. 2009) also indicated that the best gaits include push-off phases. Consequently, only the common gaits with push-off phases are analyzed in this study. The rest gaits are ignored for their atypical performance.

In human walking, the three different gaits are suitable for different environments and tasks. Gait 1 usually appears when the step length is confined to small values. Gait 3 has the maximal velocity and step length. Moreover, people of different ages exhibit variance in gait performance (e.g., double support portion, stride length and local behaviors during weight transfer) (Hollman et al. 2011; Ihlen et al. 2012). The work in this study may provide potential explanations for the gait variability.

5.2 Torque–stiffness-controlled dynamic walking versus passivity-based dynamic walking

In passivity-based bipedal walking, the walker travels down a slope completely passively or moves on a level ground with certain actuation. Purely passive walking is usually limited to one predefined pattern with no active control. To improve the practical use and further study the motion behaviors of passivity-based dynamic walking, a lot of researchers made efforts to add active control to passive walkers (Ham et al. 2007; Hosoda et al. 2008), thus the bipeds can realize periodic walking with different velocities and the walking performance can be adjusted in certain ranges (Geng et al. 2006; Mandersloot et al. 2006; Hobbelen and Wisse 2008a). In most existing passivity-based walkers, the walking performance is modulated by adjusting joint torques with fixed joint stiffness.

Introducing adaptable joint compliance (controllable joint stiffness) to passivity-based bipedal walking can broaden the accessible performance ranges (Geyer et al. 2006; Hosoda et al. 2008), improve walking efficiency (Wang et al. 2010a) and provide evidences for biological studies (Kim and Park 2011). The control space is expanded by increasing the dimensions of joint stiffness. Thus, both the external actuation and the intrinsic kinetic properties can be adjusted for walking pattern control. In this study, applying CPG-based control approach to bipedal walking is similar to adding coupling between the equilibrium positions / stiffnesses of different joints, based on basic principles of human-like walking involved in various walking patterns. Thus, the adjustments of control parameters are constrained in a particular region in the torque–stiffness space. The dimension of input is reduced and the control structure is simplified by introducing the constraint.

Figure 14 shows the difference among passivity-based walking with fixed stiffness, passivity-based walking with

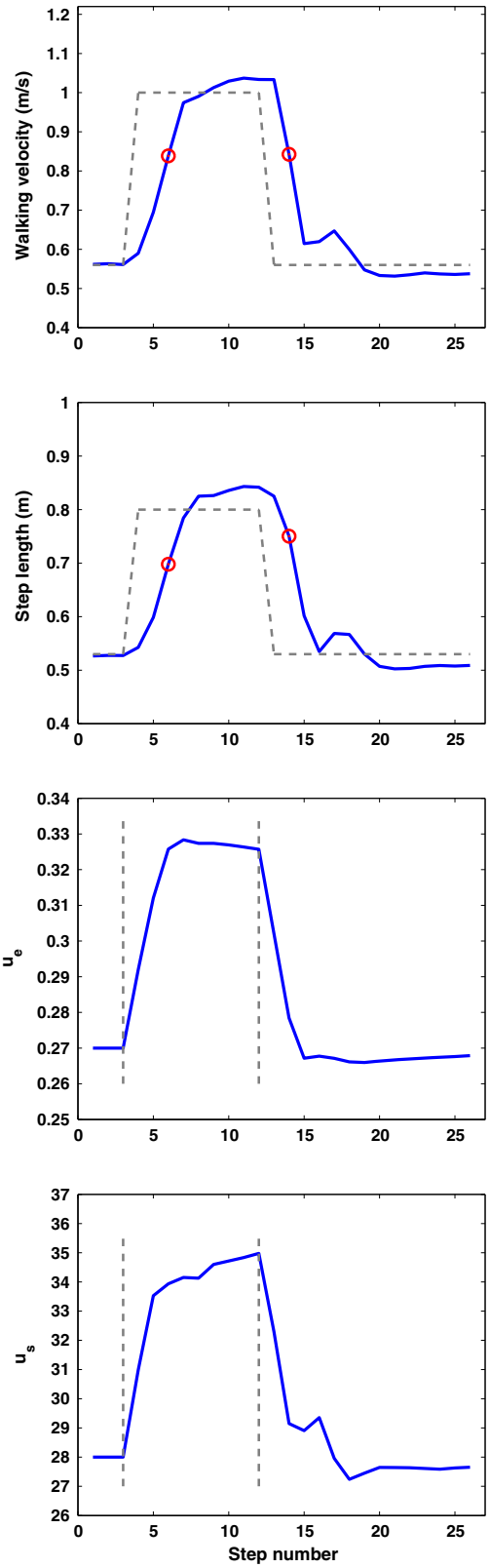

Fig. 12 Walking pattern control for gait transitions. At the end of the third step, the desired velocity is changed from 0.56 to 1.0 m/s, while the desired step length is changed from 0.53 to 0.8 m. At the end of the twelfth step, the desired velocity and step length return back to 0.56 and 0.53 m, respectively. **a** the variation of velocity, **b** the variation of step length, **c** the variation of the input signal u_e, **d** the variation of the input signal u_s. The *gray dashed lines* in **a** and **b** represents the target velocity and the target step length, respectively. The *red circles* indicate the moments of gait switching. The *gray dashed lines* in **c** and **d** describe the moment when the target walking pattern changes (Color figure online)

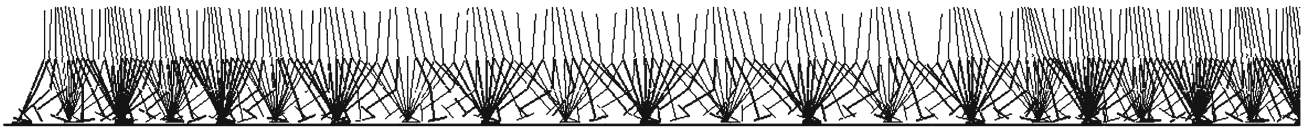

Fig. 13 The stickgrams of walking pattern transitions. The velocity and step length increase and then decrease gradually. The walker moves to gait 3 from gait 2 at the sixth step, and returns to gait 2 at the fourteenth step

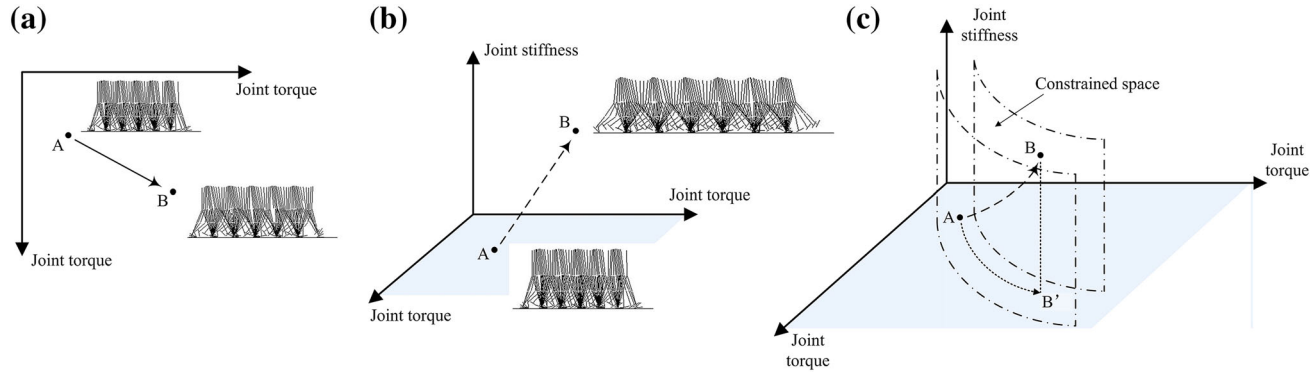

Fig. 14 Comparison of three types of passivity-based bipedal walking: **a** walking with fixed stiffness, **b** walking with adaptable stiffness, **c** torque–stiffness-controlled walking with CPGs. Each *axis* represents an input parameter (the torque or stiffness of a joint) of the mechanical system. For clarity, only two axes for joint torques and one axis for joint stiffness are plotted. Point A and point B indicate the initial and target patterns of the walking pattern transition, respectively. A stickgram of stable walking for 6 s is added to express the gait of each point in **a** and **b**. In **c**, the trajectory of walking pattern transition is constrained in the space enclosed by *dot-dash-line* surfaces. The point $B^{'}$ is the projection of B to the joint torque plane. $AB^{'}$ is constrained to a specific orbit by the coordination between joint torques. Coordination between joint stiffnesses also exists, but it is not clearly displayed since only one axis for joint stiffness is plotted in **c**

adaptable stiffness (e.g., controlled passive walking), and torque–stiffness-controlled dynamic walking with CPGs proposed in this study. The fixed-stiffness walkers are controlled by adjusting only joint torques. Hence the natural frequencies of the limbs keep constant (see Fig. 14a). For the walkers with adaptable stiffness, the natural dynamics can be adjusted during locomotion and the obtainable walking patterns are more extensive (see Fig. 14b). In the torque–stiffness-controlled walking with CPGs, the trajectories of walking pattern transitions are constrained in a specific sub-space, which is constructed based on the coordinations between the movements of each limb and feedbacks from the motion states and foot contact information (see Fig. 14c). Thus, natural and smooth walking pattern transitions can be obtained by adjusting only two parameters, and the respective effects of joint torque and joint stiffness on walking performance can be studied.

Several biological studies revealed the significance of stiffness in human walking. The tendinous tissues of the skeletal muscle serve as energy-conserving mechanisms and help improve adaptivity and efficiency in human walking and running. The mechanical energy stored in the elastic elements of muscle can be recovered as both kinetic and gravitational energy (Ishikawa et al. 2005). Human experiments indicated that an increase in leg stiffness with speed would beneficially increase the propulsion energy (Kim and Park 2011). Introducing adjustable natural frequency to bipedal walking and analyzing the respective effects of external actuation and intrinsic dynamics are also helpful in furthering our understanding of the insights of real human walking.

In existing studies, the state variables of GPG models are often chosen as the torques generated by the flexor and the extensor of each joint (Taga et al. 1991; Verdaasdonk et al. 2009). To analyze the functions of joint torque and joint stiffness separately in motion control, we employ the equilibrium position and stiffness of each joint as the CPG state variables, which is equivalent to the antagonistic muscle models in the view of dynamics.

Compliance (or impedance) control is chosen as the basis of the model in preference to alternative robot control strategies because muscles act more like tunable springs or compliance devices. Compliance control has the further advantage that it is applicable for a variety of motor tasks, and is both more robust and more simple than alternative control strategies.

5.3 The effects of joint torque and joint stiffness

Within all the obtainable stable walking cycles of our biped model, the mechanical cost of transport ranges from 0.055 to 0.179. For example, at the velocity of $Fr = 0.26$, the optimal c_{mt} is 0.78 (see Fig. 9). The values are comparable

with those of most existing passivity-based walkers (Hobbelen and Wisse 2008b; Collins et al. 2005). For steady-state walking in this study, increasing velocity and step length decreases the energetic efficiency, as also found in former studies (Hobbelen and Wisse 2008a).

Biological studies indicated that an optimal stride frequency for efficiency exists with any given speed in human normal walking (Cavagna and Franzetti 1986). However, only relatively small joint stiffness is considered in this study for the avoidance of oscillatory behaviors and chaotic gaits. The results of the proposed dynamic model validate human frequency–efficiency curve below the optimal stride frequency.

The experimental results of this study suggest that larger stiffness results in higher energetic efficiency with equal velocity. It implies that in order to achieve a larger velocity within the studied range, adjusting joint stiffness is more economical in efficiency than changing only joint torques. Large stiffness can decrease angular velocities of limbs before impacts and thus reduce the energy loss as mentioned in the previous section. Another explanation is from the view of works on CoM of the walker. With the same walking velocity, large stiffness means high step frequency and small step length, and thus leads to low energy consumption, since the rate of mechanical work performed on the CoM increases with the fourth power of step length revealed by Kuo et al. (2005).

5.4 Real-time control of velocity and step length

Several studies have investigated walking velocity control of passivity-based bipedal walkers by adjusting the external actuation. Mandersloot et al. (2006) realized transitions between different velocities in three walking models in simulation. The bipedal machine "Runbot" can walk at the velocity up to 0.8 m/s (Geng et al. 2006). The walking velocity ranges from $Fr = 0.25$ to 0.5. Hobbelen and Wisse (2008a) studied speed control of limit cycle walkers in both simulation models and the prototype "Meta". The obtained velocity of the physical prototype has a range of $Fr = 0.1$ to 0.28. Our previous study showed walking velocity transitions of the bipedal walking robot Veronica with adaptable joint stiffness (Huang et al. 2013). The achievable Fr of Veronica is from 0.07 to 0.16, which is a little smaller than other robots, caused by the limitation of the servomotor powers. In this study, the proposed torque–stiffness-controlled biped can realize walking at the speed from 0.42 to 1.2 m/s with the leg length as 0.8 m. The corresponding Fr ranges from 0.15 to 0.43. The range is wider and the general velocity is larger than those of most bipedal walking prototypes with adaptable compliant joints, since the model described in this study is relatively ideal, for example the joints are frictionless.

Real-time velocity control is realized in the proposed torque–stiffness-controlled walking with a CPG-based control method. The normalized velocity Fr transits from 0.16 to 0.23 with different control methods. The effects of joint torque and joint stiffness on speed control are separately studied. The results reveal that the advantage of adjusting actuation torques over tuning stiffness is the fast response to the variation of desired performance. It means that the effects of adjusting the natural dynamics of the mechanical system itself are embodied on the walking performance more slowly, compared with the variation of external actuation. The possible explanation may be that both positive and negative torques on the limbs are increased by increasing only the joint stiffness, thus it takes more steps to converge to the walking cycle with new natural frequency. Nevertheless, stiffness control shows benefits in fluency and accuracy. Increasing the portion of stiffness control is helpful in reducing the velocity oscillation and improving the control precision. The walking velocity changes toward the desired value smoothly with a small overshoot and a small steady-state error. The locomotion better adapts to the varied desired walking behavior by adjusting the natural dynamics of the mechanical system. In general, suitable portions of joint torque and joint stiffness adjustments can achieve the optimal performance in walking velocity control.

6 Conclusion

In this paper, we proposed a novel walking paradigm named Torque–Stiffness-Controlled Dynamic Walking, which extends the concept of Controlled Passive Walking.

A seven-link bipedal walking model is built with an upper body, two upper legs, two lower legs and flat feet. A torsional spring with adjustable equilibrium position and stiffness is mounted at each joint. Both the joint torque and the joint stiffness (represents the external actuation and the intrinsic natural dynamics, respectively) are adjustable on-line. The biologically inspired control system based on central pattern generators introduces coordination between the movements of the limbs and feedbacks according to the natural motion characteristics. The bipedal walker can perform stable walking with different gaits and realize walking gait transition in real time dependent only on two control parameters, which stand for the levels of joint torque and joint stiffness, respectively.

In the experiments, we have studied the respective effects of joint torque and joint stiffness on gait selection, walking performance and walking pattern control. The results show that both increasing joint torque and increasing joint stiffness lead to higher velocity and larger step length. Step frequency is mainly determined by joint stiffness. Joint torque has only

a minimal influence on the frequency when the step length is not very large. In walking performance control, the advantage of changing the external actuation is the fast response, while adjusting the intrinsic natural dynamics is beneficial in fluency and control accuracy. The optimal choice is the combination of these two manners. Walking pattern control with specific velocity and step length can be realized by changing joint torque and joint stiffness simultaneously.

Our study proposed a highly structured passivity-based walking paradigm with adaptable joint torque and joint stiffness. The bio-inspired CPG-based control system and the mechanical system can behave cooperatively to adapt to the desired walking performance among different gaits. The proposed bipedal locomotor system may provide insights into how people achieve efficient and flexible walking pattern switching, and suggest a new solution to motion control of bipedal robots with adaptable stiffness.

There are several ways to extend this study in the future. We intend to eliminate the chaotic gaits in the cases of large actuation, in order to extend the range of obtainable walking performance. In addition, it is worth improving the control methods to raise the accuracy in walking performance control.

Acknowledgments This work was supported by the National Natural Science Foundation of China (Nos. 61005082, 61020106005), the Beijing Nova Program (No. Z141101001814001) and the 985 Project of Peking University (No. 3J0865600).

7 Appendix

7.1 Appendix A: Lagrange's equations for the dynamic walker

The model can be defined by the Euclidean coordinates $\mathbf{r}$, which can be described by the x-coordinate and y-coordinate of the center of mass of each stick and the corresponding directions.

The walker can also be described by the generalized coordinates $\mathbf{q}$:

$$\mathbf{q} = (x_h, y_h, \theta_1, \theta_2, \theta_b, \theta_{2s}, \theta_{1f}, \theta_{2f})^{'} \tag{12}$$

We defined matrix J as follows:

$$J = \mathrm{d}\mathbf{r}/\mathrm{d}\mathbf{q} \tag{13}$$

The mass matrix in rectangular coordinate $\mathbf{r}$ is defined as:

$$M = \mathrm{diag}(m_l, m_l, I_l, m_t, m_t, I_t, m_b, m_b, I_b, m_s, m_s, I_s, m_f, m_f, I_f, m_f, m_f, I_f) \tag{14}$$

where m-components are the masses of each stick, while I-components are the moments of inertia, as shown in Fig. 1a.

The constraint function is marked as $\xi(\mathbf{q})$, which is used to maintain foot contact with ground, the direction of the upper body and knee locking. Each component of $\xi(\mathbf{q})$ should keep zero to satisfy the constraint conditions.

We can obtain the equations as following:

$$M_q\ddot{\mathbf{q}} = \mathbf{F_q} + \Phi^{'}\mathbf{F_c} \tag{15}$$

$$\xi(\mathbf{q}) = \mathbf{0} \tag{16}$$

where $\Phi = \frac{\partial \xi}{\partial \mathbf{q}}$. $\mathbf{F_c}$ is the constraint force vector. M_q is the mass matrix in the generalized coordinates:

$$M_q = J^{'}MJ \tag{17}$$

$\mathbf{F_q}$ is the active external force in the generalized coordinates:

$$\mathbf{F_q} = J^{'}\mathbf{F} - J^{'}M\frac{\partial J}{\partial \mathbf{q}}\dot{\mathbf{q}}\dot{\mathbf{q}} \tag{18}$$

where $\mathbf{F}$ is the active external force vector in the Euclidean coordinates.

For the walking model in this paper, $\mathbf{F}$ includes gravitation, the damping torques, and the joint torques generated by the torsional springs. The sum of damping torques and compliance torques are calculated by Eq. (1). Thus, the natural dynamics of the model can be adjusted by controlling joint stiffness and equilibrium positions.

Equation (16) can be transformed to the followed equation:

$$\Phi\ddot{\mathbf{q}} = -\frac{\partial(\Phi\dot{\mathbf{q}})}{\partial \mathbf{q}}\dot{\mathbf{q}} \tag{19}$$

Then the equations in matrix format can be obtained from Eqs. (15) and (19):

$$\begin{bmatrix} M_q & -\Phi^{'} \\ \Phi & 0 \end{bmatrix}\begin{bmatrix} \ddot{\mathbf{q}} \\ \mathbf{F_c} \end{bmatrix} = \begin{bmatrix} \mathbf{F_q} \\ -\frac{\partial(\Phi\dot{\mathbf{q}})}{\partial \mathbf{q}}\dot{\mathbf{q}} \end{bmatrix} \tag{20}$$

The equation of the strike can be obtained by integration of Eq. (15):

$$M_q\dot{\mathbf{q}}^{+} = M_q\dot{\mathbf{q}}^{-} + \Phi^{'}\Lambda_c \tag{21}$$

where $\dot{\mathbf{q}}^{+}$ and $\dot{\mathbf{q}}^{-}$ are the generalized velocities just after and just before the strike, respectively. Here, Λ_c is the impulse acted on the walker which is defined as follows:

$$\Lambda_c = \lim_{t^{-}\to t^{+}}\int_{t^{-}}^{t^{+}} \mathbf{F_c}\mathrm{d}t \tag{22}$$

Since the strike is modeled as a fully inelastic impact, the walker satisfies the constraint function $\xi(\mathbf{q})$. Thus, the motion is constrained by the followed equation after the strike:

$$\frac{\partial \xi}{\partial \mathbf{q}}\dot{\mathbf{q}}^{+} = \mathbf{0} \tag{23}$$

Table 2 The parameters of the oscillators for equilibrium position control

	$\tilde{u}_1^e$	w_{1j}	c_1	d_{1j}	$F_{\text{eed},1}$
Hip joint of leg 1, $i = 1$					
Phase *A*	$-u_e$	$w_{12} = -0.3,\ w_{15} = -0.05$	1	$d_{12} = 1,\ d_{15} = 1.5$	$0.02(\dot{\theta}_2 - \dot{\theta}_1)$
Phase *B*	$-u_e$	$w_{12} = -0.3,\ w_{15} = -0.05$	1	$d_{12} = 1,\ d_{15} = 1.5$	$0.02(\dot{\theta}_2 - \dot{\theta}_1)$
Phase *C*	$-u_e$	$w_{12} = -0.3,\ w_{15} = -0.05$	1	$d_{12} = 1,\ d_{15} = 1.5$	$0.02(\dot{\theta}_2 - \dot{\theta}_1)$
Phase *D*	$-u_e$	$w_{12} = -0.3,\ w_{15} = -0.05$	1	$d_{12} = 1,\ d_{15} = 1.5$	$0.02(\dot{\theta}_2 - \dot{\theta}_1)$
Phase *E*	u_e	$w_{12} = -0.3,\ w_{15} = -0.05$	1	$d_{12} = 1,\ d_{15} = 1.5$	$0.02(\dot{\theta}_2 - \dot{\theta}_1)$
Phase *F*	u_e	$w_{12} = -0.3,\ w_{15} = -0.05$	1	$d_{12} = 1,\ d_{15} = 1.5$	0
Phase *G*	u_e	$w_{12} = -0.3,\ w_{15} = -0.05$	1	$d_{12} = 1,\ d_{15} = 1.5$	0
Phase *H*	u_e	$w_{12} = -0.3,\ w_{15} = -0.05$	1	$d_{12} = 1,\ d_{15} = 1.5$	$0.02(\dot{\theta}_2 - \dot{\theta}_1)$
	$\tilde{u}_2^e$	w_{2j}	c_2	d_{2j}	$F_{\text{eed},2}$
Hip joint of leg 2, $i = 2$					
Phase *A*	u_e	$w_{21} = -0.3,\ w_{24} = -0.02,\ w_{26} = -0.05$	1	$d_{21} = 1,\ d_{24} = 0.5,\ d_{26} = 1.5$	$0.02(\dot{\theta}_1 - \dot{\theta}_2)$
Phase *B*	u_e	$w_{21} = -0.3,\ w_{24} = -0.02,\ w_{26} = -0.05$	1	$d_{21} = 1,\ d_{24} = 0.5,\ d_{26} = 1.5$	$0.02(\dot{\theta}_1 - \dot{\theta}_2)$
Phase *C*	u_e	$w_{21} = -0.3,\ w_{24} = -0.02$	1	$d_{21} = 1,\ d_{24} = 0.5,\ d_{26} = 1.5$	$0.02(\dot{\theta}_1 - \dot{\theta}_2)$
Phase *D*	u_e	$w_{21} = -0.3,\ w_{24} = -0.02$	1	$d_{21} = 1,\ d_{24} = 0.5,\ d_{26} = 1.5$	$0.02(\dot{\theta}_1 - \dot{\theta}_2)$
Phase *E*	$-u_e$	$w_{21} = -0.3$	1	$d_{21} = 1,\ d_{24} = 0.5,\ d_{26} = 1.5$	$0.02(\dot{\theta}_1 - \dot{\theta}_2)$
Phase *F*	$-u_e$	$w_{21} = -0.3,\ w_{26} = -0.05$	1	$d_{21} = 1,\ d_{24} = 0.5,\ d_{26} = 1.5$	0
Phase *G*	$-u_e$	$w_{21} = -0.3,\ w_{26} = -0.05$	1	$d_{21} = 1,\ d_{24} = 0.5,\ d_{26} = 1.5$	0
Phase *H*	$-u_e$	$w_{21} = -0.3$	1	$d_{21} = 1,\ d_{24} = 0.5,\ d_{26} = 1.5$	$0.02(\dot{\theta}_1 - \dot{\theta}_2)$
	$\tilde{u}_4^e$	w_{4j}	c_4	d_{4j}	$F_{\text{eed},4}$
Knee joint of leg 2, $i = 4$					
Phase *A*	$-u_e$	$w_{42} = -0.02,\ w_{46} = 0.02$	1	$d_{42} = 2,\ d_{46} = -1$	0
Phase *B*	$-u_e$	$w_{42} = -0.02,\ w_{46} = 0.02$	1	$d_{42} = 2,\ d_{46} = -1$	0
Phase *C*	$-u_e$	$w_{42} = -0.02,\ w_{46} = 0.02$	1	$d_{42} = 2,\ d_{46} = -1$	$0.2[-\sin\theta_1 \cdot \dot{\theta}_1 + \sin\theta_2 \cdot \dot{\theta}_2 + \sin\theta_{2s} \cdot \dot{\theta}_{2s}]$
Phase *D*	u_e	$w_{42} = -0.02,\ w_{46} = 0.02$	1	$d_{42} = 2,\ d_{46} = -1$	$0.0001(\dot{\theta}_2 - \dot{\theta}_1) - 0.003(\dot{\theta}_{2s} - \dot{\theta}_2)$
	$\tilde{u}_5^e$	w_{5j}	c_5	d_{5j}	$F_{\text{eed},5}$
Ankle joint of leg 1, $i = 5$					
Phase *A*	0	$w_{51} = 0.05$	1	$d_{51} = 0.67$	$0.02(\dot{\theta}_1 - \dot{\theta}_2)$
Phase *B*	0	$w_{51} = 0.05$	1	$d_{51} = 0.67$	$0.02(\dot{\theta}_1 - \dot{\theta}_2)$
Phase *C*	0	$w_{51} = 0.05$	1	$d_{51} = 0.67$	$0.02(\dot{\theta}_1 - \dot{\theta}_2)$
Phase *D*	0	$w_{51} = 0.05$	1	$d_{51} = 0.67$	$0.02(\dot{\theta}_1 - \dot{\theta}_2)$
Phase *E*	$-u_e$	$w_{51} = 0.05$	1.5	$d_{51} = 0.67$	$0.02(\dot{\theta}_1 - \dot{\theta}_2)$
Phase *F*	$-u_e$	$w_{51} = 0.05$	1.5	$d_{51} = 0.67$	0
Phase *G*	$-u_e$	$w_{51} = 0.05$	1.5	$d_{51} = 0.67$	0
Phase *H*	$-u_e$	$w_{51} = 0.05$	1.5	$d_{51} = 0.67$	0
	$\tilde{u}_6^e$	w_{6j}	c_6	d_{6j}	
Ankle joint of leg 2, $i = 6$					
Phase *A*	$-u_e$	$w_{62} = -0.05,\ w_{64} = 0.02$	1.5	$d_{62} = 0.67,\ d_{64} = -1$	
Phase *B*	$-u_e$	$w_{62} = -0.05,\ w_{64} = 0.02$	1.5	$d_{62} = 0.67,\ d_{64} = -1$	

Table 2 continued

	$\tilde{u}_6^e$	w_{6j}	c_6	d_{6j}
Phase *C*	$0.1rad$	$w_{64} = 0.02$	1	$d_{62} = 0.67,\ d_{64} = -1$
Phase *D*	$0.1rad$	$w_{64} = 0.02$	1	$d_{62} = 0.67,\ d_{64} = -1$
Phase *E*	$0.1rad$		1	$d_{62} = 0.67,\ d_{64} = -1$
Phase *F*	$0.1rad$	$w_{62} = -0.05$	1	$d_{62} = 0.67,\ d_{64} = -1$
Phase *G*	$0.1rad$	$w_{62} = -0.05$	1	$d_{62} = 0.67,\ d_{64} = -1$
Phase *H*	$0.1rad$		1	$d_{62} = 0.67,\ d_{64} = -1$

Table 3 The parameters of the oscillator for joint stiffness control

	$\tilde{u}_1^s$	w_{1j}^s	c_1^s	d_{1j}^s	
Hip joint of leg 1, $i = 1$					
Phase *A*	u_s	$w_{12}^s = 0.15,\ w_{14}^s = 0.1,\ w_{15}^s = 0.1,\ w_{16}^s = 0.1$	1	$d_{12}^s = d_{15}^s = 1$	
Phase *B*	u_s	$w_{12}^s = 0.15,\ w_{14}^s = 0.1,\ w_{15}^s = 0.1,\ w_{16}^s = 0.1$	1	$d_{12}^s = d_{15}^s = 1$	
Phase *C*	u_s	$w_{12}^s = 0.15,\ w_{14}^s = 0.1,\ w_{15}^s = 0.1,\ w_{16}^s = 0.1$	1	$d_{12}^s = d_{15}^s = 1$	
Phase *D*	u_s	$w_{12}^s = 0.15,\ w_{14}^s = 0.1,\ w_{15}^s = 0.1,\ w_{16}^s = 0.1$	1	$d_{12}^s = d_{15}^s = 1$	
Phase *E*	u_s	$w_{12}^s = 0.15,\ w_{15}^s = 0.1,\ w_{16}^s = 0.1$	1	$d_{12}^s = d_{15}^s = 1$	
Phase *F*	u_s	$w_{12}^s = 0.15,\ w_{15}^s = 0.1,\ w_{16}^s = 0.1$	1	$d_{12}^s = d_{15}^s = 1$	
Phase *G*	u_s	$w_{12}^s = 0.15,\ w_{15}^s = 0.1,\ w_{16}^s = 0.1$	1	$d_{12}^s = d_{15}^s = 1$	
Phase *H*	u_s	$w_{12}^s = 0.15,\ w_{15}^s = 0.1,\ w_{16}^s = 0.1$	1	$d_{12}^s = d_{15}^s = 1$	
	$\tilde{u}_2^s$	w_{2j}^s	c_2^s	d_{2j}^s	
Hip joint of leg 2, $i = 2$					
Phase *A*	u_s	$w_{21}^s = 0.15,\ w_{24}^s = 0.1,\ w_{25}^s = 0.1,\ w_{26}^s = 0.1$	1	$d_{21}^s = 1,\ d_{24}^s = 0.2,\ d_{26}^s = 1$	
Phase *B*	u_s	$w_{21}^s = 0.15,\ w_{24}^s = 0.1,\ w_{25}^s = 0.1,\ w_{26}^s = 0.1$	1	$d_{21}^s = 1,\ d_{24}^s = 0.2,\ d_{26}^s = 1$	
Phase *C*	u_s	$w_{21}^s = 0.15,\ w_{24}^s = 0.1,\ w_{25}^s = 0.1,\ w_{26}^s = 0.1$	1	$d_{21}^s = 1,\ d_{24}^s = 0.5,\ d_{26}^s = 1.7$	
Phase *D*	u_s	$w_{21}^s = 0.15,\ w_{24}^s = 0.1,\ w_{25}^s = 0.1,\ w_{26}^s = 0.1$	1	$d_{21}^s = 1,\ d_{24}^s = 0.5,\ d_{26}^s = 1.7$	
Phase *E*	u_s	$w_{21}^s = 0.15,\ w_{25}^s = 0.1,\ w_{26}^s = 0.1$	1	$d_{21}^s = 1,\ d_{26}^s = 1.7$	
Phase *F*	u_s	$w_{21}^s = 0.15,\ w_{25}^s = 0.1,\ w_{26}^s = 0.1$	1	$d_{21}^s = 1,\ d_{26}^s = 1.7$	
Phase *G*	u_s	$w_{21}^s = 0.15,\ w_{25}^s = 0.1,\ w_{26}^s = 0.1$	1	$d_{21}^s = 1,\ d_{26}^s = 1.7$	
Phase *H*	u_s	$w_{21}^s = 0.15,\ w_{25}^s = 0.1,\ w_{26}^s = 0.1$	1	$d_{21}^s = 1,\ d_{26}^s = 1.7$	
	$\tilde{u}_4^s$	w_{4j}^s	c_4^s	d_{4j}^s	
Knee joint of leg 2, $i = 4$					
Phase *A*	u_s	$w_{41}^s = 0.1,\ w_{42}^s = 0.1,\ w_{46}^s = 0.01$	0.2	$d_{42}^s = 5,\ d_{46}^s = 5$	
Phase *B*	u_s	$w_{41}^s = 0.1,\ w_{42}^s = 0.1,\ w_{46}^s = 0.01$	0.2	$d_{42}^s = 5,\ d_{46}^s = 5$	
Phase *C*	u_s	$w_{41}^s = 0.1,\ w_{42}^s = 0.1,\ w_{46}^s = 0.01$	0.5	$d_{42}^s = 2,\ d_{46}^s = 1.2$	
Phase *D*	u_s	$w_{41}^s = 0.1,\ w_{42}^s = 0.1,\ w_{46}^s = 0.01$	0.5	$d_{42}^s = 2,\ d_{46}^s = 1.2$	
	$\tilde{u}_5^s$	w_{5j}^s	c_5^s	d_{5j}^s	$F_{\text{eed},5}^s$
Ankle joint of leg 1, $i = 5$					
Phase *A*	u_s	$w_{51}^s = 0.1,\ w_{52}^s = 0.1$	1	$d_{51}^s = 1$	$5(\dot{\theta}_{1f} - \dot{\theta}_1)$
Phase *B*	u_s	$w_{51}^s = 0.1,\ w_{52}^s = 0.1$	1	$d_{51}^s = 1$	$5(\dot{\theta}_{1f} - \dot{\theta}_1)$
Phase *C*	u_s	$w_{51}^s = 0.1,\ w_{52}^s = 0.1$	1	$d_{51}^s = 1$	$5(\dot{\theta}_{1f} - \dot{\theta}_1)$
Phase *D*	u_s	$w_{51}^s = 0.1,\ w_{52}^s = 0.1$	1	$d_{51}^s = 1$	$5(\dot{\theta}_{1f} - \dot{\theta}_1)$
Phase *E*	u_s	$w_{51}^s = 0.1,\ w_{52}^s = 0.1$	1	$d_{51}^s = 1$	$5(\dot{\theta}_{1f} - \dot{\theta}_1)$

Table 3 continued

	$\tilde{u}^s_5$	w^s_{5j}	c^s_5	d^s_{5j}	$F^s_{\text{eed},5}$
Phase F	u_s	$w^s_{51}=0.1,\ w^s_{52}=0.1$	1	$d^s_{51}=1$	$5(\dot{\theta}_{1f}-\dot{\theta}_1)$
Phase G	u_s	$w^s_{51}=0.1,\ w^s_{52}=0.1$	1	$d^s_{51}=1$	$5(\dot{\theta}_{1f}-\dot{\theta}_1)$
Phase H	u_s	$w^s_{51}=0.1,\ w^s_{52}=0.1$	1	$d^s_{51}=1$	$5(\dot{\theta}_{1f}-\dot{\theta}_1)$
	$\tilde{u}^s_6$	w^s_{6j}	c^s_6	d^s_{6j}	$F^s_{\text{eed},6}$
Ankle joint of leg 2, $i=6$					
Phase A	u_s	$w^s_{61}=0.1,\ w^s_{62}=0.1,\ w^s_{64}=0.01$	1	$d^s_{62}=1,\ d^s_{64}=0.2$	$10(\dot{\theta}_{2f}-\dot{\theta}_{2s})$
Phase B	u_s	$w^s_{61}=0.1,\ w^s_{62}=0.1,\ w^s_{64}=0.01$	1	$d^s_{62}=1,\ d^s_{64}=0.2$	$10(\dot{\theta}_{2f}-\dot{\theta}_{2s})$
Phase C	u_s	$w^s_{61}=0.1,\ w^s_{62}=0.1,\ w^s_{64}=0.01$	0.6	$d^s_{62}=1.7,\ d^s_{64}=0.83$	0
Phase D	u_s	$w^s_{61}=0.1,\ w^s_{62}=0.1,\ w^s_{64}=0.01$	0.6	$d^s_{62}=1.7,\ d^s_{64}=0.83$	0
Phase E	u_s	$w^s_{61}=0.1,\ w^s_{62}=0.1$	0.6	$d^s_{62}=1.7$	0
	$\tilde{u}^s_6$	w^s_{6j}	c^s_6	d^s_{6j}	$F^s_{\text{eed},6}$
Phase F	u_s	$w^s_{61}=0.1,\ w^s_{62}=0.1$	0.6	$d^s_{62}=1.7$	0
Phase G	u_s	$w^s_{61}=0.1,\ w^s_{62}=0.1$	0.6	$d^s_{62}=1.7$	0
Phase H	u_s	$w^s_{61}=0.1,\ w^s_{62}=0.1$	0.6	$d^s_{62}=1.7$	0

Then the equation of strike in matrix format can be derived from Eqs. (21) and (23):

$$\begin{bmatrix} M_q & -\Phi' \\ \Phi & 0 \end{bmatrix} \begin{bmatrix} \dot{\mathbf{q}}^+ \\ \Lambda_c \end{bmatrix} = \begin{bmatrix} M_q \dot{\mathbf{q}}^- \\ \mathbf{0} \end{bmatrix} \tag{24}$$

Parameters

$m_b = 12.0\,\text{kg}$, upper body mass
$m_t = 2.5\,\text{kg}$, thigh mass
$m_s = 2.5\,\text{kg}$, shank mass
$m_f = 1.2\,\text{kg}$, foot mass
$I_b = 0.36\,\text{kg m}^2$, moment of inertia of upper body
$I_t = 3.33 \cdot 10^{-2}\,\text{kg m}^2$, moment of inertia of thigh
$I_s = 3.33 \cdot 10^{-2}\,\text{kg m}^2$, moment of inertia of shank
$I_f = 4.0 \cdot 10^{-3}\,\text{kg m}^2$, moment of inertia of foot
$l_b = 0.6\,\text{m}$, upper body length
$l_t = 0.4\,\text{m}$, thigh length
$l_s = 0.4\,\text{m}$, shank length
$l_f = 0.2\,\text{m}$, foot length
$r = 0.3$, foot ratio, which is defined as the ratio of the distance between the heel and the ankle to whole foot length
$g = 9.81\,\text{ms}^{-2}$, gravitational acceleration

7.2 Appendix B: Parameters of central pattern generators

Parameters of oscillators for equilibrium position

The parameter values of an unit oscillator controlling the equilibrium position [as shown in Eq. (7)]:

$\tau_1 = \tau_2 = \tau_3 = \tau_4 = 0.02$,
$\tau_5 = \tau_6 = 0.05$.
$\tau_1' = \tau_2' = \tau_3' = \tau_4' = 0.01$,
$\tau_5' = \tau_6' = 0.02$.
$\beta = 0.005$.

The expressions of $\tilde{u}^e_i$ and $F_{\text{eed},i}$ and the values of w_{ij}, c_i and d_{ij} in each phase of different joints are listed in Table 2 (suppose leg 1 is the stance leg).

It is worth mentioning that not all the terms of w_{ij} and d_{ij} are listed in the tables. The absent terms are taken to be zero. The column for feedback is not included in the table if there is no feedback at the corresponding joint. The knee joint of the stance leg in all the phases and the knee joint of the swing leg in phase E, F, G and H are locked, and the corresponding degrees of freedom are thus taken off, the parameters of joint 4 in phase E, F, G and H and joint 3 are not listed in the above tables.

Parameters of oscillators for stiffness

The parameter values of an unit oscillator controlling the joint stiffness [as shown in Eq. (8)]:

$\tau^s_i = 1,\ \tau'^s_i = 0.2, \quad i = 1, 2, \ldots, 6$
$\beta^s = 0.02$.

The expressions of $\tilde{u}^s_i$ and $F^s_{\text{eed},i}$ and the values of w^s_{ij}, c^s_i and d^s_{ij} in each phase of different joints are listed in Table 3 (suppose leg 1 is the stance leg).

Similar to the case of equilibrium position control, not all the terms of w^s_{ij} and d^s_{ij} for stiffness control are listed in the tables. The absent terms are taken to be zero. The column for feedback is not included in the table if there is no feedback at the corresponding joint. Similarly, due to knee locking, the parameters of joint 4 in phase E, F, G and H and joint 3 are not listed in the above tables.

References

Amemiya M, Yamaguchi T (1984) Fictive locomotion of the forelimb evoked by stimulation of the mesencephalic locomotor region in the decerebrate cat. Neurosci Lett 50:91–96

Cazalets JR, Borde M, Clarac F (1995) Localization and organization of the central pattern generator for hindlimb locomotion in newborn rat. J Neurosci 15:4943–4951

Cavagna GA, Franzetti P (1986) The determinants of the step frequency in walking in humans. J Physiol 373:235–242

Chevallereau C, Djoudi D, Grizzle JW (2008) Stable bipedal walking with foot rotation through direct regulation of the zero moment point. IEEE Trans Robot 24:390–401

Collins S, Wisse M, Ruina A (2001) A three-dimensional passive-dynamic walking robot with two legs and knees. Int J Robot Res 20:607–615

Collins S, Ruina A, Tedrake R, Wisse M (2005) Efficient bipedal robots based on passive-dynamic walkers. Science 307:1082–1085

Delvolve I, Branchereau P, Dubuc R, Cabelguen JM (1999) Fictive rhythmic motor patterns induced by NMDA in an in vitro brain stem–spinal cord preparation from an adult urodele. J Neurophysiol 82:1074–1077

Frigo C, Crenna P, Jensen LM (1996) Moment–angle relationship at lower limb joints during human walking at different velocities. J Electromyogr Kines 6:177–190

Fukuoka Y, Habu Y, Fukui T (2013) Analysis of the gait generation principle by a simulated quadruped model with a CPG incorporating vestibular modulation. Biol Cybern 107:695–710

Geng T, Porr B, Worgotter F (2006) Fast biped walking with a sensor-driven neuronal controller and real-time online learning. Int J Robot Res 25:243–259

Geyer H, Seyfarth A, Blickhan R (2006) Compliant leg behaviour explains basic dynamics of walking and running. Proc R Soc B 273:2861–2867

Hobbelen DGE, Wisse M (2008a) Controlling the walking speed in limit cycle walking. Int J Robot Res 27:989–1005

Hobbelen DGE, Wisse M (2008b) Ankle actuation for limit cycle walkers. Int J Robot Res 27:709–735

Hollman JH, McDade EM, Petersen RC (2011) Normative spatiotemporal gait parameters in older adults. Gait and Posture 34:111–118

Hosoda K, Takuma T, Nakamoto A, Hayashi S (2008) Biped robot design powered by antagonistic pneumatic actuators for multi-modal locomotion. Robot Auton Syst 56:46–53

Huang Y, Wang Q, Chen B, Xie G, Wang L (2012) Modeling and gait selection of passivity-based seven-link bipeds with dynamic series of walking phases. Robotica 30:39–51

Huang Y, Vanderborght B, Van Ham R, Wang Q, Van Damme M, Xie G, Lefeber D (2013) Step length and velocity control of a dynamic bipedal walking robot with adaptable compliant joints. IEEE-ASME Trans Mechatron 18:598–611

Huang Y, Wang Q (2012) Gait selection and transition of passivity-based bipeds with adaptable ankle stiffness. Int J Adv Robot Syst 9:99–110

Ihlen EAF, Sletvold O, Goihl T, Wik PB, Vereijken B, Helbostad J (2012) Older adults have unstable gait kinematics during weight transfer. J Biomech 45:1559–1565

Ijspeert AJ, Crespi A, Ryczko D, Cabelguen JM (2007) From swimming to walking with a salamander robot driven by a spinal cord model. Science 315:1416–1420

Ijspeert AJ (2008) Central pattern generators for locomotion control in animals and robots: a review. Neural Netw 21:642–653

Ishikawa M, Komi PV, Grey MJ, Lepola V, Bruggemann G (2005) Muscle–tendon interaction and elastic energy usage in human walking. J Appl Physiol 99:603–608

Ker RF, Alexander RMcN, Bennett MB (1988) Why are mammalian tendons so thick? J Zool Lond 216:309–324

Kim S, Park S (2011) Leg stiffness increases with speed to modulate gait frequency and propulsion energy. J Biomech 44:1253–1258

Kim Y, Tagawa Y, Obinata G, Hase K (2011) Robust control of CPG-based 3D neuromusculoskeletal walking model. Biol Cybern 105:269–282

Kormushev P, Ugurlu B, Calinon S, Tsagarakis NG, Caldwell DG (2011) Bipedal walking energy minimization by reinforcement learning with evolving policy parameterization. In: Proceedings of the IEEE/RSJ international conference on intelligent robots and systems, San Francisco, USA

Kuo AD, Donelan JM, Ruina A (2005) Energetic consequences of walking like an inverted pendulum: step-to-step transitions. Exerc Sport Sci Rev 33:88–97

Li C, Lowe R, Ziemke T (2012) Modelling walking behaviors based on CPGs: a simplified bio-inspired architecture. LNAI 7426:156–166

Mandersloot T, Wisse M, Atkeson CG (2006) Controlling velocity in bipedal walking: a dynamic programming approach. In: Proceedings of the IEEE-RAS international conference on humanoid robots, Genoa, Italy

McGeer T (1990) Passive dynamic walking. Int J Robot Res 9:68–82

Or J (2009) A hybrid CPG–ZMP controller for the real-time balance of a simulated flexible spine humanoid robot. IEEE Trans Syst Man Cybern Part C Appl Rev 39:547–561

Owaki D, Osuka K, Ishiguro A (2008) On the embodiment that enables passive dynamic bipedal running. In: Proceedings of the IEEE international conference on robotics and automation, Pasadena, CA, USA

Owaki D, Kano T, Tero A, Akiyama M, Ishiguro A (2012) Minimalist CPG model for inter- and intra-limb coordination in bipedal locomotion. In: Proceedings of international conference on intelligent autonomous systems, Jeju, South Korea

Perry J (1992) Gait analysis. SLACK Inc, Thorofare, NJ

Suzuki S, Furuta K, Hatakeyama S (2005) Passive walking towards running. Math Comp Model Dyn 11:371–395

Taga G, Yamaguehi Y, Shimizu H (1991) Self-organized control of bipedal locomotion by neural oscillators in unpredictable environment. Biol Cybern 65:147–159

Tlalolini D, Chevallereau C, Aoustin Y (2009) Comparison of different gaits with rotation of the feet for a planar biped. Robot Auton Syst 57:371–383

Ugurlu B, Saglia JA, Tsagarakis NG, Caldwell DG (2012) Hopping at the resonance frequency: a trajectory generation technique for bipedal robots with elastic joints. In: Proceedings of the IEEE international conference on robotics and automation, Saint Paul, USA

Wang Q, Huang Y, Wang L (2010a) Passive dynamic walking with flat feet and ankle compliance. Robotica 28:413–425

Wang Q, Huang Y, Zhu J, Wang L, Lv D (2010b) Effects of foot shape on energetic efficiency and dynamic stability of passive dynamic biped with upper body. Int J Hum Robot 7:295–313

Wang WJ, Crompton RH (2004) Analysis of the human and ape foot during bipedal standing with implications for the evolution of the foot. J Biomech 37:1831–1836

Weiss PL, Kearney RE, Hunter IW (1986a) Position dependence of ankle joint dynamics-I. Passive mechanics. J Biomech 19:727–735

Weiss PL, Kearney RE, Hunter IW (1986b) Position dependence of ankle joint dynamics-II. Active mechanics. J Biomech 19:737–751

Wisse M, Hobbelen DGE, Schwab AL (2007) Adding an upper body to passive dynamic walking robots by means of a bisecting hip mechanism. IEEE Trans Robot 23:112–123

Vanderborght B, Van Ham R, Verrelst B, Van Damme M, Lefeber D (2008) Overview of the lucy project: dynamic stabilization of a biped powered by pneumatic artificial muscles. Adv Robot 22:1027–1051

Van Ham R, Sugar TG, Vanderborght B, Hollander KW, Lefeber D (2009) Compliant actuator designs review of actuators with passive

adjustable compliance/controllable stiffness for robotic applications. IEEE Robot Autom Mag 16:81–94

Van Ham R, Vanderborght B, Van Damme M, Verrelst B, Lefeber D (2007) MACCEPA, the mechanically adjustable compliance and controllable equilibrium position actuator: design and implementation in a biped robot. Robot Auton Sys 55:761–768

Vanderborght B, Van Ham R, Lefeber D, Sugar TG, Hollander KW (2009) Comparison of mechanical design and energy consumption of adaptable, passive-compliant actuators. Int J Robot Res 28:90–103

Vanderborght B, Albu-Schaeffer A, Bicchi A, Burdet E, Caldwell DG, Carloni R, Catalano M, Eiberger O, Friedl W, Ganeshd G, Garabini M, Grebenstein M, Grioli G, Haddadina S, Hoppnera H, Jafari A, Laffranchi M, Lefeber D, Petit F, Stramigioli S, Tsagarakis N, Van Damme M, Van Ham R, Visser LC, Wolf S (2013) Variable impedance actuators: a review. Robot Auton Sys 61:1601–1604

Verdaasdonk BW, Koopman HFJM, Van Der Helm FCT (2009) Energy efficient walking with central pattern generators: from passive dynamic walking to biologically inspired control. Biol Cybern 101:49–61